Exciton Dynamics in Tetracene Single Crystals Studied Using Femtosecond Laser Spectroscopy

by

Zephania Birech

Dissertation approved for the degree of

Doctor of Philosophy

at the University of Stellenbosch

Department of Physics,
University of Stellenbosch,
Private Bag X1, 7602 Matieland, South Africa.

Promoters:

Prof. Heinrich Schwoerer

Prof. Erich G. Rohwer

December 2012

Declaration

By submitting this dissertation electronically, I declare that the entirety of the work contained therein is my own, original work, that I am the sole author thereof (save to the extent explicitly otherwise stated), that reproduction and publication thereof by Stellenbosch University will not infringe any third party rights and that I have not previously in its entirety or in part submitted it for obtaining any qualification.

Date: December, 2012 .....

Abstract

Exciton Dynamics in Tetracene Single Crystals Studied Using Femtosecond Laser Spectroscopy

Zephania Birech

Department of Physics,
University of Stellenbosch,
Private Bag X1, 7602 Matieland, South Africa.

Dissertation: PhD

December 2012

In recent years academic and industrial interest on π-conjugated organic semiconductors has increased due to their electrical and optical properties that can be applied in devices such as organic light emitting diodes (OLED), organic field-effect transistors (OFET), organic solar cells (OSC) among others. Majority of research was focused on device design rather than understanding the fundamental processes responsible for the observed properties. Such knowledge can be useful in tailoring new compounds exhibiting desired properties. Optical characterization was one of the ways to extract this information. In this work, steady state absorption and femtosecond transient absorption spectroscopy measurements were done on tetracene single crystals and tetracene in toluene solvent at room temperature. A lot of previously reported work was on polycrystalline thin films and few on free standing crystals. In this study, single crystals of thicknesses 200 nm, 300 nm and 500 nm were cut using a microtome. The steady state absorption spectra of these crystals revealed existence of two non-degenerate first excited singlet states (S_1) that can be excited with orthogonally polarized optical fields, $\perp$ b and $\parallel$ b axis of the ab face of the unit cell respectively. A Davydov splitting of between 0.08 eV and 0.12 eV between the two states was determined and compared well with literature values implying similarities in the samples.

The transient absorption measurements done at room temperature on tetracene dissolved in toluene solvent displayed a broad positive signal implying that excited state absorption (ESA) plays a major role. For the first time signatures of excited triplet absorption were seen 20 ps after excitation at 2.67 eV (465 nm) and was proposed to result from ultrafast inter-system crossing (ISC) facilitated by the position of the second excited triplet state T_2 being energetically below the first excited singlet state S_1. The overlapping signals in the transient absorption spectra of single crystals in the UV to VIS regime frustrated efforts to interpret

them in the past but here we employed a robust deconvolution technique involving sum of Gaussian functions fit. From this we were able to identify a number of important properties which include

1. Singlet exciton fission occurs on sub-picoseconds through direct fission of higher-lying singlet states forming two triplets $S_n \rightarrow 2T_1$, and at 40 ps timescales through the thermally activated singlet fission of the lowest excited singled state $S_1 \rightarrow 2T_1$. These were seen on positive signals decaying beyond 2.6 ns attributed to absorption by T_1 state at 2.66 eV (467 nm) and at 2.5 eV (496 nm). The attribution of the former was done for the first time here while the latter had been done in other studies elsewhere on polycrystalline thin films [1].

2. The rapid generation of triplets was independent of excitation energy. This was because the same timescales, sub-ps and 40 ps, were obtained from excitation done at 3.20 eV (387 nm) and at 2.34 eV (530 nm). This was contrary to the expectation of the often used model where exciton fission from the S_1 state excited at 530 nm proceeds only at around 40 - 100 ps and not at shorter time scales.

3. The high energy Davydov exciton at 2.47 eV (503 nm) was short-lived as it readily undergoes fission forming triplet excitons. This was revealed through probing the excited crystal with field polarized $\perp$ *b*-axis of the *ab* face of the unit cell. Such measurements had never been reported before as thin enough single crystals were unavailable.

4. There was a short lived ($<$10 ps) emission from the low energy Davydov at around 2.30 eV (540 nm). The emission was followed by a weak positive signal attributed to trapped excitons at defect sites and which exhibited a decay extending beyond 2 ns.

Uittreksel

Exciton Dynamics in Tetracene Enkellopend Crystals bestudeer Met behulp van Femtoseconde Laser Spektroskopie

("Exciton Dynamics in Tetracene Single Crystals Studied Using Femtosecond Laser Spectroscopy")

Zephania Birech

Fisika Departement,
Universiteit van Stellenbosch,
Privaatsak X1, 7602 Matieland, Suid Afrika.

Proefskrif: PhD

Desember 2012

Onlangs het akademiese en industriële belangstelling van π-gekonjugeerde organiese semi-geleiers toegeneem as gevolg van hulle elektriese en optiese eienskappe wat toegepas kan word in toestelle soos organiese liguitstralende diodes, organiese veld-effek transistors en organiese sonselle. 'n Meerderheid van die navorsing is gefokus op die ontwerp van toestelle eerder as om die begrip van die fundamentele prosesse te verstaan wat verantwoordelik is vir die waargenome eienskappe. Sodanige kennis kan nuttig wees in die aanpassing van nuwe materie om verlangde eienskappe te genereer. Optiese karakterisering is een van die maniere om hierdie inligting te onttrek. In hierdie werk word stabielestaat absorpsie en femtosekonde absorpsie spektroskopie metings gedoen op enkelkristal tetracene in n tolueen oplosmiddel by kamertemperatuur. Baie van vorheen gerapporteerde werk was van poly-kristal dun films en net 'n paar op vrystaande kristalle. In hierdie studie is enkel-kristalle met diktes van 200 nm, 300 nm en 500 nm gesny. Die stabielestaat absorpsie spektra van hierdie kristalle het die bestaan ãâvan twee nie-gedegenereerde eerste opgewekte enkel toestande (S1) bewys, wat opgewek kan word met ortogonale gepolariseerde lig wat onderskeidelik loodreg en parallel met betrekking tot die a-b gesig van die eenheidsel is. 'n Davydov splitsing van tussen 0.08 eV en 0.12 eV tussen die twee toestande is bepaal en vergelyk goed met die literatuur waardes.

Die femtosekonde absorpsie metings wat gedoen is by kamertemperatuur op tetracene opgelos in 'n tolueen oplosmiddel vertoon 'n wye positiewe sein. Dit impliseer dat opgewekte toestand absorpsie 'n belangrike rol speel. Vir die eerste keer is tekens van opgewekte triplet toestand absorpsie gesien, 20 ps na die opwekking met 2,67 eV (465 nm) lig. Die verskynsel was voorgestel as ultra-vinnige inter-stelsel kruising wat gefasiliteer word deur die posisie van die tweede opgewekte triplet toestand (T2) wat energiek onder die eerste opgewekte enkel toestand (S1)

is. Die oorvleueling van seine in die femtosekonde absorpsie spektra het die interpretasie in die verlede moeilik gemaak maar hier het ons van 'n robuuste dekonvolusie tegniek, wat die som van verskillende Gauss funksies pas, gebruik gemaak. Hieruit was ons in staat om van die belangrikste eienskappe te identifiseer wat die volgende ingesluit het:

1. Enkel eksiton splyting kom voor op sub-pikosekondes deur onmiddellike splyting van hoërliggende enkel toestande wat twee triplet toestande vorm, en op die 40 ps tydskaal, deur die termies geaktiveerde splyting van die laagste opgewekte enkel toestand. Dit is gesien deur positiewe seine wat verval na 2.6 ns, toegeskryf aan absorpsie deur die T1 toestand van 2.66 eV (467 nm) en 2.5 eV (496 nm). Die toeskrywing van die eerste proses is hier vir die eerste keer gedoen, terwyl die laasgenoemde gedoen is in ander studies elders op poly-kristal films.

2. Die vinnige generasie van triplets was onafhanklik van opwekende energie. Dit was omdat die dieselfde tye, sub-ps en 40 ps, ââverkry is uit opwekking met 3.20 eV (387 nm) en 2.34 eV (530 nm). Dit was in strydig met die dikwels gebruikte model waar eksiton splyting van die S1 staat opgewek met 530 nm ongeveer 40 - 100 ps vat en nie op korter tydskale nie.

3. Die leeftyd van die hoërenergie Davydov eksiton by 2.47 eV (503 nm) was kort, aangesien dit graag splyting na triplet eksitone ondergaan. Dit was gewys deur die kristal met lodreg gepolariseerde lig met repsek tot die a-b gesig van die eenheidsel te ondersoek. Sulke metings was nog nooit aangemeld nie aangesien dun genoeg enkel kristalle nie beskikbaar was nie.

4. Daar was 'n kort duurende (<10 ps) emissie van die lae energie Davydov by ongeveer 2.30 eV (540 nm). Die emissie is gevolg deur 'n swak positiewe sein wat toegeskryf word aan vasgevangde eksitone by onsuiwerhede in die kristal en wat 'n verval wat buite 2 ns strek.

Acknowledgements

There are a number of people that made it possible for me to successfully perform my research. First and foremost the advice, guidance, encouragements and patience of my promoters Prof. Heinrich Schwoerer and Prof. Erich Rohwer. There are no enough words to express my gratitudes for all they have done for me which also includes sourcing for my scholarship and funding my PhD studies. I promise to make good use of the knowledge and skills obtained under their guidance in making the society better and more better. I also thank all the ultra-fast science group members including Gurthwin, Monty, Kerstin, Nic, Illana, David and Olufemi who were always ready to help in one way or another. In particular Kerstin and Gurthwin helped me learn Labview programme and Olufemi for using Gausian programme to model tetracene molecules. Illana and Kerstin also helped in cutting of the crystals using microtome. I thank them all.

I would not have had a chance to research on molecular crystals if it were not for Prof. Jens Pflaum of university of Wuerzburg for kindly growing and supplying the tetracene crystals. I am so thankful for that. I am also grateful for Prof. Markus Schwoerer of University of Bayreuth for hosting me in Germany and giving valuable suggestions and contributions regarding the results obtained from my studies on the crystal. I thank him for arranging a meeting with Prof. Hans Baesler who gave me very forward answers regarding questions I had on the obtained transient absorption spectroscopy studies results of tetracene. It was a honor and kind of him to grant his time to me. I very much enjoyed my short stay in Germany and miss the good German cuisine prepared by Mrs. Hannelore Schwoerer.

There are people you cannot forget in life because of their encouragement and advice. One of such people who also inspire me is Prof. Thomas Feurer of University of Bern, Switzerland. He hosted me in his institute where I learned a lot. His donation of some laser equipment to my home university in Kenya cannot go un-mentioned. I also appreciate the kindness of Prof. Peter Hamm of university of Zurich for his time in explaining to me the concepts of 2D spectroscopy and accepting my visit to his labs.

I cannot forget to thank the Laser Research Institute for accepting me as a postgraduate student and providing equipment for my research. Many thanks also goes to African Laser Center (ALC) for the scholarship.

My studies were made a success due to being surrounded by loving people. I do not have enough words to thank my wife, Salome for taking care of our three lovely children Qurie, Madelyne and Alfa while I was away studying in South Africa. I appreciate their understanding and encouragements. I am fortunate to have had very loving and hard working parents, the late Mr. and Mrs. Kibirech

Mining, who made sure that we received enough education despite our very low economic status. I thank the church and the entire Kerotet community for the many fund raising done for my school and college fees. I also cannot forget my brothers, sisters and relatives who always encouraged me.

Contents

List of Figures

List of Tables

1. Introduction

Over the last two decades molecules with conjugated π-electron systems have become a source of novel organic-based devices which include organic light-emitting diodes (OLEDs) [2] and organic field-effect transistors (OFETs) [3, 4, 5]. They are now gaining a new interest in the solar cell industry for their potential to improve significantly the efficiency of photovoltaic solar cells [6, 7, 8]. A lot of research is also on-going in trying to understand the mechanisms and timescales of energy and charge transfer in the naturally occurring π-conjugated molecular system, the photosynthetic light harvesting complex, found in various living organisms (higher plants, algae, bacteria e.t.c) [9, 10, 11]. The ability of these natural light harvesters to capture and efficiently channel excitation energy over considerable distances (tens of nanometers) has been the compelling motivation to study them. The goal has been to understand the precise molecular principles governing the high light-to-charge conversion efficiency ($>$ 95 %) [11] and applying it in the synthesis of artificial molecular complexes mimicking the process of photosynthesis. This will in turn set the stage for using light harvesting to fuel renewable energy technologies [10].

Carbon atoms are the main structural elements in π-conjugated molecular systems. The electron configuration of an isolated carbon atom in its ground state is $1s^2 2s^2 2p^2$. In a molecule it's valence is four due to the four electrons in the outermost shell. The four orbital electrons can form four bonds (equivalent hybridized sp^3 bonds) in a non-conjugated organic molecule such as methane [12]. In conjugated organic molecules i.e having alternating single and double bonds (see Figure 1.2 (a)), a double bond can form between two carbon atoms due to sp^2 hybridization. Here, three degenerate orbitals are constructed out of one s and two p orbitals leaving one p orbital [13] as schematically shown in figure 1.1. This remaining p (the p_z) orbitals form a π bond which results from the overlap of the p-orbitals above and below the plane of the ring (see Figure 1.2(b,c)). The three sp^2 orbitals which lie in one plane and are separated by 120^o angle form the so called σ bonds. These bonds form single bonds. The electrons in the σ bonds are not free (i.e more localized) compared to the π bonds' electrons which may be delocalized over all or part of the molecule. As can be seen in Figure 1.2(b,c) showing the distribution of π-electrons on the lowest un-occupied molecular orbitals (LUMO) and on the highest occupied molecular orbitals (HOMO) or ground state in tetracene, the π-orbitals are out of plane of the atoms and so can interact with each other freely and become delocalized. The π bonds lie on a plane that is perpendicular to that of the σ bonds. A double bond consists of a σ-bond and a π-bond.

Among molecular structures with conjugated π-electron systems are molecular crystals. These are solids in which organic molecules are held together in

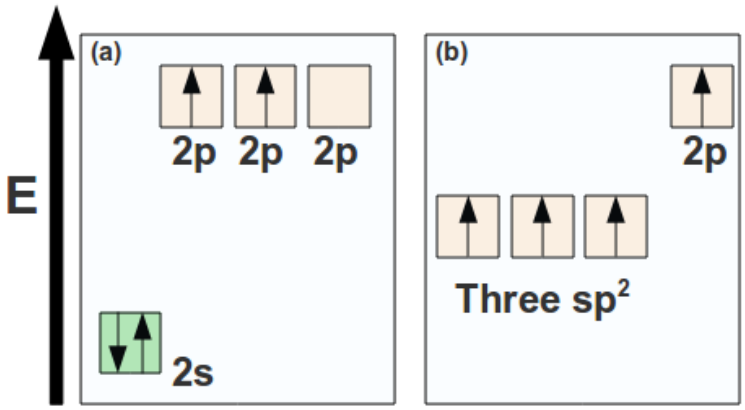

Figure 1.1: A schematic of sp^2 hybridization in carbon. (a)The orbitals of a free carbon atom showing the upper two shells $2s^2 2p^2$ which play a role in bonding. (b) sp^2 hybridization brought about by bonding of two carbon atoms. This result in an sp^2 hybridized orbital where one of the 2s orbital electron is shared with those of two 2p orbitals leaving one 2p orbital electron. The remaining p orbital can form a π-bond.

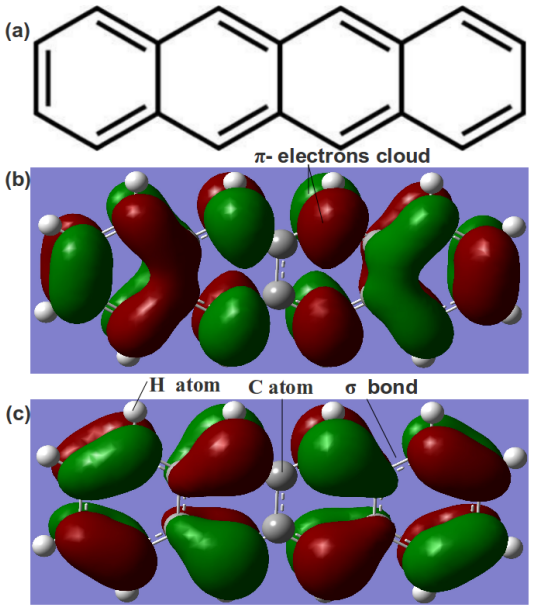

Figure 1.2: (a)Molecular structure of conjugated compound tetracene consisting of four fused benzene rings and (b) the distribution of the π-electron cloud in the lowest unoccupied molecular orbital (LUMO) and (c) the distribution in the highest occupied molecular orbital (HOMO). The colors represent the different phases $(+, -)$ of the cloud with respect to the σ bonds' plane. These were calculated using Gausian programme.

position by weak intermolecular forces (Van der Waals forces). These forces result from fluctuating charge distributions which induces dipole moments in the neighboring molecules. Due to the weak intermolecular interactions, the molecules in the crystal retain their individual physical properties, hence the term molecular. The low melting temperature (e.g 217 ^{o}C for Anthracene compared with 937^{o}C for Germanium [13]), low mechanical strength and high compressibility can also be attributed to the same weak forces. This also explains why several different lattice arrangements with similar ground state energies (polymorphism)

are common in these crystals. Many of their optical properties which include low electronic excitation energies (a few eV), absorption and luminescence in the visible, near-infrared or ultraviolet spectral regimes can be attributed to the π orbitals of the individual constituents [13]. The arrangement of molecules in their crystal's unit cells result in anisotropy in optical, electrical, magnetic and mechanical properties [14, 15]. The interaction of N differently oriented molecules in the unit cell upon excitation cause splitting of electronic terms into N states that can be excited by light of different polarizations respectively. This splitting is referred to as Davydov splitting [13, 14, 16, 17]. Examples of organic molecular crystals include polyacenes (e.g anthracene, tetracene, pentacene, pyrene e.t.c), radical ion salts, polymers (e.g PVC) among many [13].

Energy conduction in molecular crystals is by means of excitons [13]. These are bound electron-hole (e-h) pairs formed upon excitation that move within the crystal [18, 13, 12] and can release energy radiatively (photoluminescence) when they recombine [19]. The e-h pairs that are localized on the same molecule are referred to as Frenkel excitons [13] and play a key role in energy transport in molecular crystals, polymers and biological systems. Those pairs that are delocalized over several molecules and separated by a large distance between them are termed Mott-Wannier excitons and are mainly created in inorganic semiconductors such as Gallium Arsenide. The pairs where the hole is formed on one molecule and the electron on the adjacent one are called charge transfer (CT) excitons. Among Frenkel excitons are singlet and triplet excitons. A Singlet exciton is formed when the promoted electron retains its spin in the excited state such that the total quantum spin of the molecule is zero i.e $\mathbf{S}$=0. Triplet excitons on the other hand are created when the excited electron undergoes a spin inversion in the excited state resulting in total quantum spin $\mathbf{S}$=1 [13, 20].

The definitive positions and lifetimes of singlet and triplet exciton states in the larger polyacenes such as tetracene and pentacene are still debatable. The lowest band of the first excited singlet state (S_1) in tetracene at room temperature for instance has been stated to be at 2.30 eV (540 nm) [21] and 2.40 eV (517 nm) [22] in single crystals and 2.32 eV (533 nm) [23] and 2.34 eV (530 nm) [1] in polycrystalline thin films. Its lifetime was between 200 ps [24] to 300 ps [25] in polycrystalline thin films and single crystals respectively and 20 ns to 23 ns [26] in solution. The absorptivity of molecular crystals are generally high, in the order of 10^5 cm^{-1} [13] and so very dilute solution or nanometer thick crystals were needed. Virtually all the reported results on single crystals involved use of thick samples ($\gg$1 μm) where electro-absorption and fluorescence measurements were done [22, 25, 27, 28, 29, 30]. The main reason of using such thick crystals was lack of technology to produce good quality thin free standing single crystals. In polycrystalline thin films, the different orientations of crystallites on the substrate was likely to frustrate the resolution of some weak signals such as those due to transitions in the triplet states in transient absorption measurements [23] besides making it hard to perform polarized probing of the excited sample.

One of the tasks of this research was to prepare free standing single crystals from the provided thick ($\approx$ 500 μm) sublimation grown tetracene crystal platelets. This involved first estimating the appropriate thickness for performing transmission measurements from absorbance values obtained from sample in solution.

Slicing of the platelets using a microtome and obtaining nanometer thick samples was then to be done. The samples were to be supported on a copper wire mesh with squares of dimensions 150 μm.

Since tetracene crystallizes in a layered herringbone structure with a triclinic unit cell consisting of two non-equivalent molecules under translational operation [13, 14, 16, 31, 32], two excitonic states that can be excited with orthogonally polarized light were expected. The energy splitting of these states (Davydov splitting) results from the electrostatic interaction of the two transition dipole moments [13, 31]. The energetic positions of these two excitonic states and the amount of splitting in our single crystals were to be determined and compared with values obtained in literature. The solution to crystal shift energy resulting from non-resonant interaction of the excited molecules with neighbouring ground state molecules was also to be estimated.

Femtosecond transient absorption measurements on free standing single tetracene crystals are few in literature, the author of this work came across only one in reference [33]. From such measurements, ultra-fast energy transfer between states in the same molecule or between neighbouring molecules are studied. The information obtained is useful in developing technological appliances utilizing these properties. Of particular interest in the solar cell industry for instance is the fast generation of two triplet excitons from one singlet exciton (singlet fission) which has been shown theoretically to improve the efficiency of solar cells by a factor of 1.5 (from 31% to 46%) [6, 34]. In this study transient absorption measurements using femtosecond laser pulses were performed on the obtained single tetracene crystals using the setup built in our lab. The experimental transient absorption setup was first made spectrally tunable over a wide band of frequencies ranging from the UV to the VIS regime. This necessitated the building and characterization of a non-collinear parametric amplifier (NOPA). When the setup was ready transient absorption data was obtained and analyzed. From the results, transient states were identified and interpreted. Given that the measurements were performed in the UV-VIS regime of the electromagnetic spectrum where there are overlap of different excited states, a method to deconvolve them was established.

This dissertation has been organized as follows.

Chapter 1 introduces the general concept of π-conjugated molecular systems, the general properties of molecular crystals and the aims and objectives of this work.

Chapter 2 provides a brief description of the properties and applications of tetracene crystals which includes crystal structure, Davydov splitting, excitonic processes and superradiance.

Chapter 3 discusses the steady state absorption measurements on both tetracene in solution and single crystals. The vibrational bands in the $S_0 \rightarrow S_1$ transitions are identified and compared in both solution and crystal samples. A description of Davydov splitting determination is given.

Chapter 4 discusses femtosecond transient absorption measurements performed on solution and crystal samples. A number of transient states are identified and interpreted.

Conclusions are then given in the fifth chapter.

2. Structure and Optical Properties of Tetracene crystals

In this dissertation we deal with the optical properties of molecular crystals with emphasis on tetracene which is one of the linear polyacenes. The other members of this group are naphthalene, anthracene and pentacene consisting of two, three and five fused benzene rings respectively. Tetracene has four. These molecules crystallize in a layered herringbone structure with two molecules per unit cell. The information which can be obtained experimentally includes exciton band splitting (Davydov splitting), exciton creation and decay time scales and their interactions. The occurrence of superradiance which is characterized by shortening of radiative lifetimes of excitons at lower temperatures can also be studied. A brief description of these properties together with their potential applications is given in this chapter.

Single crystals

A single crystal is a solid with a continuous lattice, unbroken up to the edges and with no grain boundaries. Tetracene crystallizes in a layered herringbone structure whose unit cell is triclinic with two molecules. A herringbone crystal structure is one in which the molecules lie above the valleys/gaps of the neighboring molecules as shown in Figure 2.1. This arrangement enables maximum

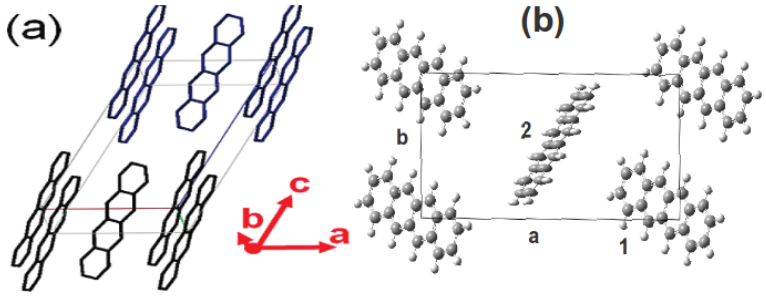

Figure 2.1: The tetracene crystal structure showing (a) the herringbone arrangement of the molecules in tetracene unit cell (adapted from [21]) and (b)the crystal structure as viewed from the ab face with the two translationally inequivalent molecules in the unit cell labeled 1 and 2.

intermolecular interactions and optimum packing in space. Naphthalene, anthracene and pentacene crystals also prefers this structural arrangement [13]. The molecules in these crystals have no permanent dipoles but have charge distributions that fluctuate with time resulting in fluctuating dipole moments in the

neighboring molecules. The net effect is the weak attractive *Van der Waals force* which is responsible for holding molecules together in molecular crystals [13]. The geometry (sizes of the three edge lengths a, b, c and the three interaxial angles, α, β, γ) of the unit cell of a crystal is normally used to classify or group crystal structures into cubic, hexagonal, tetragonal e.t.c. Naphthalene and anthracene for instance are monoclinic (with $a \neq b \neq c$ and $\alpha = \beta = 90^o \neq \gamma$) while tetracene and pentacene are triclinic (with $a \neq b \neq c$ and $\alpha \neq \beta \neq \gamma \neq 90^o$). The dimensions of the unit cells of these four molecular crystals have been given in Table 2.1. The length of dimension c and the unit cell volume V can be seen to increase proportionately with increase in number of benzene rings in the molecule. These crystals typically expose a wide ab (001) face which is the accessible face for optical measurements [14].

Table 2.1: Table of unit cell geometrical dimensions of naphthalene, anthracene, tetracene and pentacene crystals [13, 31]. Z represent the number of molecules in a unit cell and V its volume. Two crystal structures are shown; monoclinic and triclinic.

Crystal	Naphthalene	Anthracene	Tetracene	Pentacene
Structure	monoclinic	monoclinic	triclinic	triclinic
a(Å)	8.24	8.56	7.90	7.90
b(Å)	6.00	6.04	6.03	6.06
c(Å)	8.66	11.16	13.53	16.01
$\alpha\ (^o)$	90	90	100.3	101.9
$\beta\ (^o)$	122.9	124.7	113.2	112.6
$\gamma\ (^o)$	90	90	86.3	85.8
V(Å^3)	360	474	583	692
Z	2	2	2	2
Benzene rings	2	3	4	5

Davydov Splitting

In molecular crystals the molecules are held together by weak intermolecular interactions, the Van der Waals forces. What happens to the energy states of a free isolated molecule when they interact forming the crystal? A detailed description was given by Davydov [35] and we shall only concentrate on the main points relevant in this work.

To illustrate the consequence of intermolecular interactions on the energy states of the individual isolated molecules in the crystal, a dimer (two coupled molecules) is considered. In the absence of interaction due to a large separation distance the two molecules such as those of tetracene in gas or solution phase (tetracene monomers) have their respective ground $|\phi_1\rangle, |\phi_2\rangle$ and excited $|\phi_1^*\rangle, |\phi_2^*\rangle$ states with energies $E_{\phi_1} = E_{\phi_2} = E_g$ and $E_{\phi_1^*} = E_{\phi_2^*} = E^*$ respectively as schematically depicted in Figure 2.2. When the two are in close proximity such that their wavefunctions ϕ_1, ϕ_2 and ϕ_1^*, ϕ_2^* in the ground and excited states mix (overlap), a dimer is formed with three states $|\phi_G\rangle$, $|\phi_-^*\rangle$ and $|\phi_+^*\rangle$ that are shifted in energy relative to those of the monomer (see Figure 2.2). These dimer states have energies

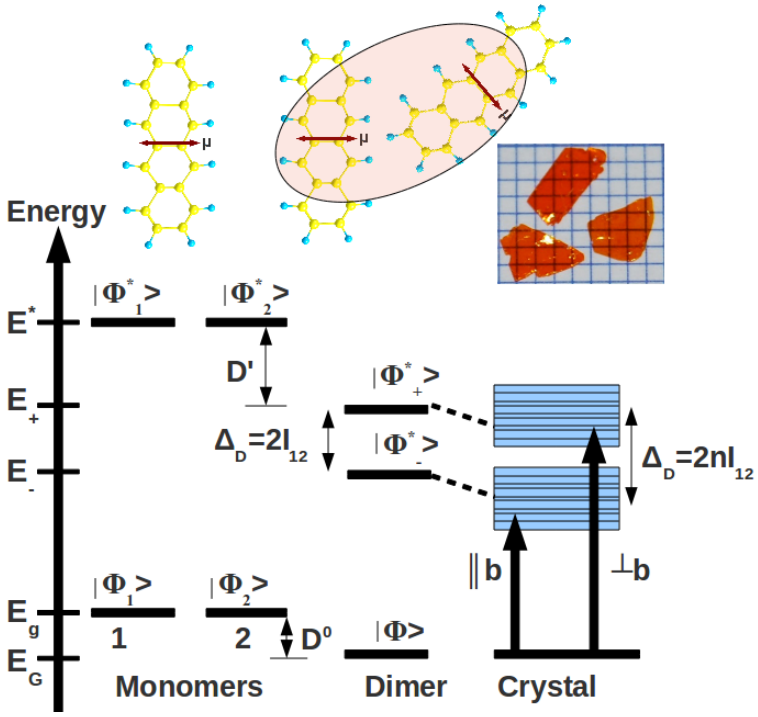

Figure 2.2: A schematic of Davydov splitting in a dimer and in a crystal. 1 and 2 represent two isolated molecules such as those of tetracene in gas or solution phase with respective ground and excited states. At close proximity, Coulomb interaction causes splitting of the states by twice the interaction energy I_{12} (i.e $2I_{12}$). The quantity $\triangle_D$ is called Davydov splitting. $D^{'}$ and D^0 are the Coulomb interaction energy in the excited and ground state respectively. In the crystal, splitting results in a band [13] and the case shown here represents a crystal with n interacting molecules resulting in splitting nI_{12}.

E_G, E_- and E_+ respectively. Besides the lifting of degeneracy in excited states, non-resonant interaction of the excited dimer with the neighboring un-excited molecules result in energy shift $D = D^{'} - D^0$ from those of the monomer [13]. $D^{'}$ represents the Coulomb interaction energy in the excited state i.e Coulomb interaction of the charge distribution of the excited state in molecule 1 with that of the ground state of molecule 2. This can be expressed as [13, 35]

$$D^{'} = \langle \phi_1^* | V_{12} | \phi_2 \rangle = \langle \phi_2^* | V_{12} | \phi_1 \rangle \tag{2.1}$$

and Coulomb interaction in the ground state D^0 expressed as

$$D^0 = \langle \phi_1 | V_{12} | \phi_2 \rangle = \langle \phi_2 | V_{12} | \phi_1 \rangle, \tag{2.2}$$

where V_{12} is the interaction Hamiltonian that depends on the coordinates of the electrons of the interacting molecules. It should be noted that the dimers' excited states depicted in Figure 2.2 exists only when one of the molecule is excited and the other is in the ground state. When both are excited simultaneously, then the dimer's electronic population will evolve in the so called doubly excited state (not shown in Figure 2.2) situated above $|\phi_-^*\rangle$ and $|\phi_+^*\rangle$ [36]. This latter state is not relevant in our current discussion. The wavefunctions of the singly excited dimer (i.e to either of the two excited states $|\phi_-^*\rangle$ and $|\phi_+^*\rangle$) is a linear combination

[13]

$$\phi^*_{\pm} = \frac{1}{\sqrt{2}}(\phi^*_1\phi_2 \pm \phi_1\phi^*_2) \tag{2.3}$$

and the energies of the two dimer states are given by

$$E_{\pm} = E_{mol} + D \pm 2I_{12} \tag{2.4}$$

where $E_{mol} = E^* - E_g$, is the molecular excitation energy, E^* and E_g are the monomer excited and ground state energies respectively and I_{12} is the resonance interaction energy which describes exchange of excitation energy between molecules 1 and 2(Figure 2.2). The quantity $2I_{12}$ is the Davydov splitting energy.

In the crystal, the dimer states $|\phi^*_-\rangle$ and $|\phi^*_+\rangle$ form bands [13, 35] as schematically shown in Figure 2.2. The wavefunctions of these bands can be expressed as [35]

$$\phi^c_{\pm}(k) = \frac{1}{\sqrt{2}}(\psi^c_1(k) \pm \psi^c_2(k)) \tag{2.5}$$

with energy

$$E^c_{\pm}(k) = E_{mol} + D^* + I_{11}(k) \pm I_{12}(k). \tag{2.6}$$

Here, $\psi^c_{1,2}(k)$ are the wave functions of the two differently oriented molecules in the crystal's unit cells, D^* is the static gas to crystal shift and is in general < 0 since an excited molecule interacts more strongly with the adjacent molecules than an unexcited one (this leads to a decrease of the excitation energy of the crystal)[13, 35] and $k = 2\pi/\lambda$ is the magnitude of the wavevector $\mathbf{k}$. $I_{11}(k)$ and $I_{12}(k)$ represent the resonant interactions between translationally equivalent and non-equivalent molecules in the crystal respectively. This means that apart from proximity, relative orientation of the molecules also determines the degree of Davydov splitting i.e value of $2nI_{12}$ [36]. If for instance the crystal consist of only one molecule per unit cell such as that of Hexamethylbenzene [13] then equation 2.6 can be expressed as

$$E^c(k) = E_{mol} + D^* + I_{11}(k). \tag{2.7}$$

Since the molecules in the crystal's unit cell have the same orientation i.e they are translationally equivalent, then there is no Davydov splitting. The interactions between adjacent molecules (with interaction energy $I_{11}(k)$) result in non-degenerate states differing only by the value of the wavevector k. These states in a large crystal constitute a band as consecutive values of k differ little from one another [35]. Each of the excited states defined by k collectively constitute an excited state of the whole crystal.

When there are two translationally inequivalent molecules per unit cell, then two bands of excited states are formed. The band splitting for a fixed value of the wave vector k can then be expressed by [13, 35]

$$\triangle_D = |E^c_+(k) - E^c_-(k)| = 2I_{12}(k). \tag{2.8}$$

When there are n nearest neighbor translationally inequivalent molecules in the unit cell then we have

$$\triangle_D = 2nI_{12}(k). \tag{2.9}$$

Due to the different orientations of the two molecules in the unit cell (i.e translationally inequivalent) such as in tetracene the optical transitions to the two bands, the high and the low energy Davydov, have different polarizations, $\parallel b$ and $\perp b$ respectively. The short axis b of the ab face of the crystal is used as a reference in describing polarization [14]. The origin of these polarized transitions can be visualized by considering electrostatic interaction of two transition dipole moments μ_1 and μ_2 as sketched in figure 2.3. The two dipoles can be arranged parallel or obliquely with respect to each other [37, 13].

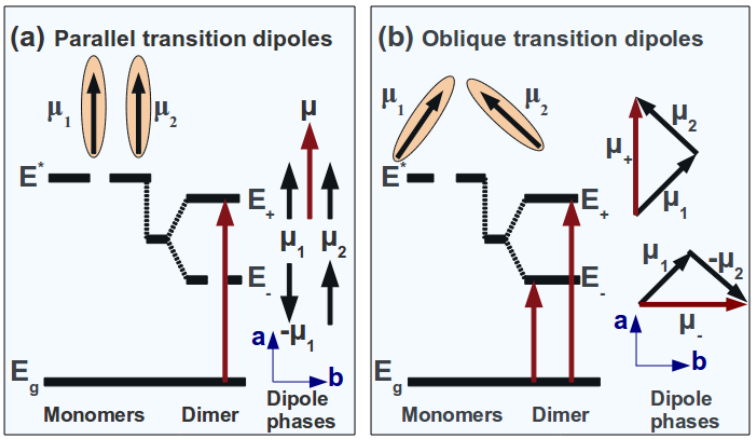

Figure 2.3: A schematic of dipole-dipole interactions with (a) parallel dipoles where interaction results in only one allowed optical transition and (b) oblique dipoles where interactions result in two states with polarized optical transitions ($\parallel b$ and $\parallel a$) .

The transition dipole moments of the individual molecules can be expressed as [13]

$$\mu_1 = \langle \phi_1 | e\mathbf{r} | \phi_1^* \rangle \tag{2.10}$$
$$\mu_2 = \langle \phi_2 | e\mathbf{r} | \phi_2^* \rangle. \tag{2.11}$$

For the dimer we have

$$\begin{aligned} \mu_\pm &= \langle \phi_G | e\mathbf{r} | \phi_\pm^* \rangle \\ &= \frac{1}{\sqrt{2}} \langle \phi_1\phi_2 | e\mathbf{r} | \phi_1\phi_2^* \pm \phi_1^*\phi_2 \rangle \\ &= \frac{1}{\sqrt{2}} \langle \phi_1\phi_2 | e\mathbf{r} | \phi_1\phi_2^* \rangle \pm \langle \phi_1\phi_2 | e\mathbf{r} | \phi_1^*\phi_2 \rangle \\ &= \frac{1}{\sqrt{2}} (\mu_1 \pm \mu_2). \end{aligned} \tag{2.12}$$

If the transition dipole moments of the two molecules are parallel i.e translationally equivalent, then one of the two optical transitions is allowed as depicted in Figure 2.3(a). From equation 2.12 one then obtains

$$\mu_+ = \frac{1}{\sqrt{2}} 2\mu_1 \text{ or } \mu_+ = \frac{1}{\sqrt{2}} 2\mu_2 \tag{2.13}$$

and the forbidden transition represented by dipole

$$\mu_{-} = 0. \tag{2.14}$$

For the case of oblique arrangement of the two transition dipole moments as depicted in Figure 2.3(b) i.e translationally inequivalent molecules, then both of the excited states have allowed transitions. These transitions as in the case of polyacenes such as anthracene and tetracene are orthogonal i.e $\parallel b$ and $\parallel a$ axis of the ab face of the crystal (see Figure 2.3(b)). Equation 2.12 represents this situation in a dimer.

This dipole-dipole interaction described above applied to singlet state ($S_0 \rightarrow S_n$) transitions. Triplet state splitting also occur but is weaker compared to those of singlets. For example a Davydov splitting (DS) of 21.5 cm^{-1} in triplets compared to 220 cm^{-1} in singlets have been reported in anthracene [13].

Davydov splitting can be determined experimentally through absorption measurements where the crystal is excited at normal incidence to the ab crystal plane with a field whose polarization with respect to the b-axis of the crystal can be varied and absorbance determined. The difference (in energy) between the center of the vibrational peaks of the spectrum obtained with field polarized $\parallel b$ and that with field polarized $\perp b$ is the Davydov splitting energy. The value of this energy for the 0-0 vibrational peak ranges from $\sim$ 200 cm^{-1} in anthracene [16], $\sim$ 630 cm^{-1} (0.08 eV) in tetracene [16, 14] and $\sim$ 1100 cm^{-1} in pentacene [16]. The other thing that should be mentioned is that DS is a crystal effect requiring lattice periodicity and vanishes in a randomly oriented system since the average over resonance interaction energies is zero [38].

Exciton processes and energy conduction in molecular crystals

One of the most important property of molecular crystals as mentioned earlier is that upon optical excitation bound electron-hole (e-h) pairs known as excitons are created [12, 13, 18]. The primary function of these electrically neutral quasiparticles are to store and transport excitation energy from one point to the next within the crystal lattice [13]. Many of the optical and optoelectronic properties in molecular crystals are determined by them and are classified basing on the distance between the electron and the hole and on their locations. Those excitons with electron and hole separation distance smaller than the unit cell dimensions and are localized on the same molecule are termed *Frenkel excitons*. These types excitons (i.e Frenkel excitons) are mainly created in molecular crystals. They are the reason why molecular crystals are considered model systems for investigating energy conduction in biological systems such as photosynthetic light harvesting complexes. If the e-h separation distance is larger than the unit cell size (about 40-100 Å) and are delocalized over several molecules then the generated excitons are called *Mott-Wannier excitons*. These latter excitons exists in inorganic crystals such as Cu_2O, Silicon or Germanium [13]. When an excitation results in transfer of an electron or hole to a molecule in the neighborhood then a *charge transfer (CT) exciton* is formed. The e-h distance in CT excitons is one

or two times greater than the unit cell size and are essential in the development of excitonic solar cells [18]. A schematic of these excitons are given in Figure 2.4.

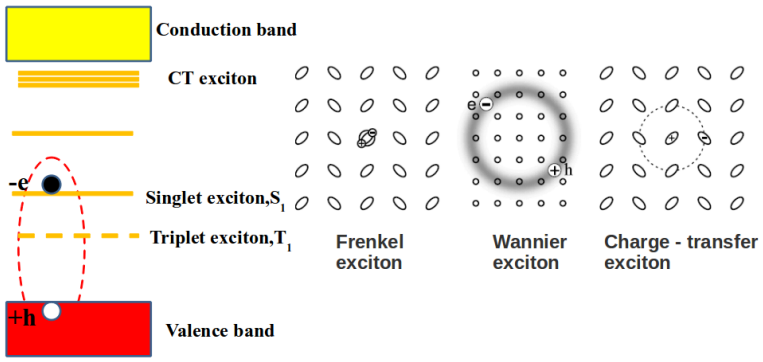

Figure 2.4: A schematic showing generation of Frenkel excitons and the different types of excitons. Among Frenkel excitons are singlet (S) and triplet (T) excitons (see text for their description). Charge transfer (CT) excitonic states are normally located just below the conduction band. Adapted from [13].

Frenkel excitons are further classified basing on the total quantum spin **S** of the excited molecule. A Singlet (S) exciton is formed when the promoted electron retains its spin in the excited state such that the total quantum spin of the molecule is zero i.e **S**=0. Triplet (T) excitons on the other hand are created when the excited electron undergoes a spin inversion in the excited state resulting in total quantum spin **S**=1 [13, 20]. These quasi-particles have a decay lifetime i.e the time taken for the electron and the hole to recombine, and diffusion lengths which can be considerably long. Some of the reported decay lifetimes and diffusion lengths of these excitons have been summarized in Table 2.2. These were obtained from references [13, 25, 29, 30].

Table 2.2: Table of decay lifetimes and diffusion lengths of the lowest singlet S_1 and triplet T_1 excitonic states and ionization energies for naphthalene, anthracene and pentacene crystals at room temperature obtained from [13, 25, 29, 30] .

Crystal	Decay lifetime (ns)		Diffusion length (Å)		Ionization energy (eV)
	S_1	T_1	S_1	T_1	
Naphthalene	10^2	5×10^8	10^2		5.0
Anthracene	20	4×10^7	10^3	10^5	4.1
Tetracene	0.3	2×10^5	120	4000	3.7

It is evident from the table that decay lifetimes and diffusion lengths of triplet excitons are considerably higher than those of singlets. This property is the reason molecular crystals are gaining interest in the photovoltaic industry where possibilities of harvesting triplet excitons to generate free positive and negative charge carriers are being explored [6, 34, 39, 40]. From the table it can be seen that singlet and triplet decay lifetimes together with ionization energies decrease with increasing conjugation length of the crystal.

The other excitonic processes includes singlet-singlet exciton annihilation or fusion which occurres at high excitation energies. This involves singlets colliding

with each other due to their high density leading to excitation of higher singlet (S_n) states or deactivation without emission of radiation but exciting phonons v in the lattice or ejection of an electron from the crystal according to the scheme [13]

$$\begin{aligned} S_1 + S_1 &\rightarrow S_n + S_0 \text{ higher excited singlet states} \\ &\rightarrow S_1 \rightarrow S_0 + v \text{ de-activation with no light emission and energy released as heat} \\ &\rightarrow e^- + h^+ \text{ electron-hole separation, ionization.} \end{aligned} \tag{2.15}$$

The opposite process to the above occurring in select organic molecules is singlet exciton fission (SF) [6, 39, 41]. This is where an organic dimer (e.g tetracene unit cell which has two differently oriented molecules) in an excited singlet state shares its excitation energy with a neighbouring ground state dimer and both are converted into triplet excited states as schematically depicted in figure 2.5[41].

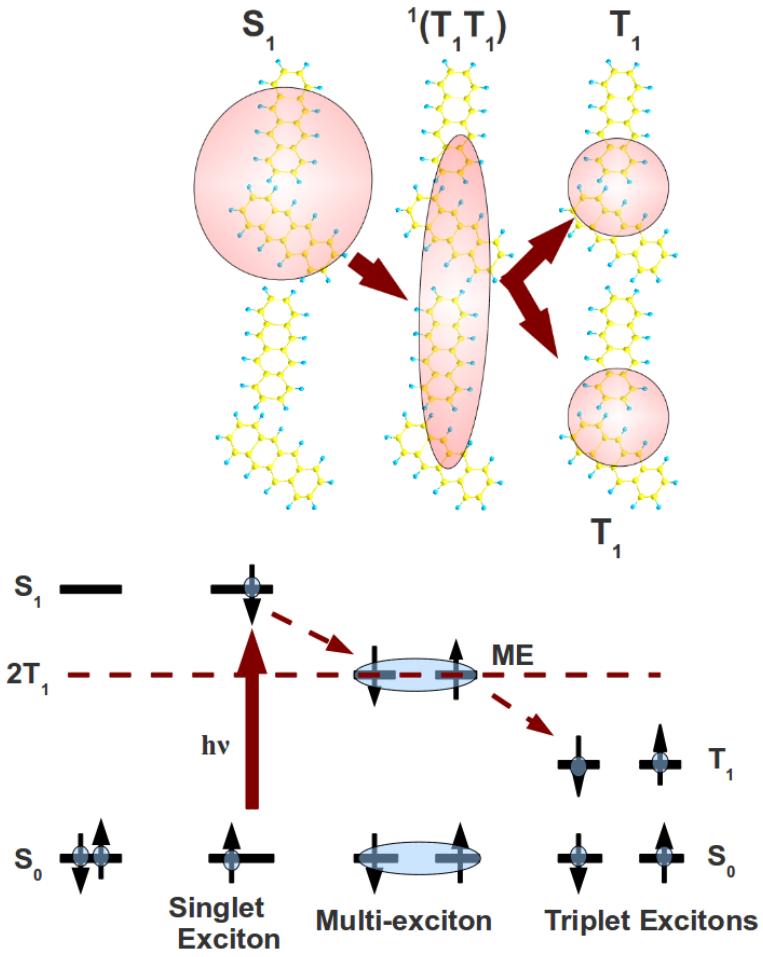

Figure 2.5: A schematic showing singlet exciton fission. Singlet excitons (S_1) created e.g in tetracene, undergoes fission producing two triplet excitons that are coupled into a pure singlet state $^1(T_1T_1)$. The two formed triplets in the multi-exciton (ME) state which is at twice the first excited triplet state energy E($2T_1$) then diffuse apart and get localized on individual dimers (or molecules [39]).

The phenomenon is a spin allowed process since the two resulting triplet excitons $^1(T_1T_1)$ are born coupled into a pure singlet state before diffusing apart (see Equation 2.16 and Figure 2.5). It can therefore be viewed as a special kind of internal conversion (IC) (transitions between states of the same multiplicity) hence can happen on an ultrafast timescale (femtoseconds to picoseconds) and competes with vibrational relaxation [39]. The two electrons in the optically inaccessible intermediate state cannot couple to the ground state via a one-electron dipole operator. This state is referred to as a multi-exciton (ME) or dark state [41, 42] and is positioned at twice the first excited triplet energy E($2T_1$). The two triplets formed from one singlet exciton soon diffuse apart and get localized on individual dimers as schematically shown in Figure 2.5. The process can also be represented in an equation of the form [13, 39, 41];

$$S_0 + S_1 \rightleftharpoons^1 (T_1T_1) \rightleftharpoons T_1 + T_1. \tag{2.16}$$

The generation of more than two triplet states has not been observed so far. For SF to occur, certain conditions must be fulfilled which includes:

1. The energy of the first singlet excited state S_1 must be equal or greater than twice the energy of the first triplet excited state T_1 i.e $E(S_1) \geq 2E(T_1)$ [1, 23, 33, 34, 39]. This condition is met very infrequently in many compounds thus making SF rare to observe. In most organic molecules twice the triplet excitation energy, $2E(T_1)$ exceeds singlet excitation energy, $E(S_1)$ significantly and so SF does not take place. The condition is, however, met in some organic molecular crystals where SF has been observed. The reported values of $E(S_1) - 2E(T_1)$ are -1.3 eV, -0.55 eV, -0.21 eV and 0.11 eV in naphthalene, anthracene, tetracene and pentacene respectively [33, 42]. From these values, it is obvious that SF is energetically allowed in pentacene. In tetracene, however, a additional energy is needed for the condition to be met. This can be provided through thermal activation and at room temperature this is readily possible [23, 33, 42].

2. There have to be at least two excitation sites to accommodate the created triplet excitations for SF to occur. Therefore, this process is not expected to happen in single small molecules at the usual energies [39].

3. It is not easy to observe SF unless if the formed triplet excitons diffuse apart rapidly as they can destroy each other by Triplet-Triplet annihilation (the reverse process shown in equation 2.16 above) usually forming an excited singlet which decays radiatively to the ground state (delayed fluorescence, DF) or a higher excited Triplet (excited triplet-triplet absorption) or resulting in the ground state singlet (phosphorescence). This annihilation can be represented in an equation of the form [13, 43];

$$\begin{aligned} T_1 + T_1 &\rightarrow S_0 + T_n \rightarrow S_0 + T_1 \quad \text{Triplet quenching} \\ &\rightarrow S_0 + S_n \rightarrow S_0 + S_1 \quad \text{delayed fluorescence.} \end{aligned} \tag{2.17}$$

S_n and T_n refers to higher electronically excited singlet and triplet states respectively. In triplet quenching, two triplets combine to produce a higher

level triplet T_n which relaxes back to the lowest level one triplet T_1. From this latter state, light emission (phosphorescence) or radiationless decay occurs.

Observation of delayed fluorescence (DF) proves that triplets were formed [13, 43, 23]. This can be observed after switching off the excitation. The intensity of DF produced by triplet-triplet annihilation can be influenced by an applied magnetic field [13, 43]. In the pair state $^1(T_1T_1)$ (or the multi-exciton state), the two triplets repeatedly collide before reacting and the possible spin correlations have both triplet as well as singlet character. The triplets in this state can be influenced by an applied magnetic field via the Zeeman interaction of the coupled individual spins with the field.

Singlet fission has been found to be of significance in improving the efficiency of dye-sensitized photovoltaic (PV) solar cells by a factor of 1.5 (from 31% to 46%) in theoretical studies done elsewhere [6, 34]. The generated two triplets from one photon must diffuse quickly to the crystal wall and be injected to a semiconductor such as a TiO_2 nanoparticle film where two electron-hole (e-h) pairs are produced. The resulting hole must be transported quickly to a hole conducting material such as Iodide ion or a hole conducting polymer [6] to avoid e-h recombination. Studies on the possibility of singlet fission being applied in water splitting to generate Hydrogen are also being done elsewhere [40].

Superradiance

Superradiance refers to a process in which the excited molecules (N molecules) co-operatively emit radiation in phase with each other (coherent light) with intensity proportional to N^2 leading to the shortening of the radiative lifetime and line narrowing of the transition [44, 45]. The emitted radiation is directional unlike in incoherent emission such as spontaneous emission where also the intensity is proportional to the number of emitting molecules (N). This phenomena, which is enhanced at lower temperatures, has been reported in tetracene (Tc) nano-aggregates and films deposited on glass substrates [45], Tc films deposited on a highly oriented pyrolytic graphite [19] and on Tc single crystals [44]. Time-resolved photoluminescence spectroscopy [19, 44, 45] and fluorescence measurements [19] were used in these studies. From these studies exciton delocalization of $\simeq$ 40 molecules in single crystals [44],$\simeq$ 10 molecules in films [45] were estimated and thus making them interesting for quantum optical applications. The fact that the molecular exciton lifetime can be varied/controlled by varying temperature [19, 45] may be useful in developing strategies for the design of organic laser diodes [19].

3. Steady state absorption measurements of tetracene

Knowledge of structure and excitonic states involved in energy transfer processes in an optically active material are vital in designing devices that optimally utilize its properties. Here we seek to establish energy positions (in wavelengths) of the excited singlet excitonic states in both tetracene crystal and solution phase samples through performing steady state absorption measurements. Steady state absorption spectra of single crystals which are rare to find in literature due to their high absorbance are provided. We also report how nanometer thick free standing single crystals that enabled us to perform these measurements were obtained.

3.1 Solution phase tetracene

Steady state absorption measurements provides a means to establish the positions of the lowest accessible electronic excited states (or excitonic states) of the sample. The simplest sample to begin with, in case the experimental setup was not designed for gas phase samples, is one in solution. In this studies tetracene was dissolved in toluene solvent. In literature, a range of solvents have been used including benzene [26, 46], acetonitrile, methanol, ethanol and 1-butanol [47] and toluene [23]. No special reason informed our choice of the solvent.

Due to the π-conjugation in tetracene molecules their optical response was expectedly high and only a small concentration was required to obtain a solution with high optical density. This was prepared by dissolving 0.0004 g of crystals in 0.37 cm^3 of toluene at room temperature obtaining a concentration of 3.1 $\times 10^{18}$ molecules / cm^3. This sample was put in a 1 mm path length quartz cuvette for performing steady state absorption measurements. The layout of the experimental set up sketched in Figure 3.1(a) was the same one used for performing transient absorption measurements whose details are discussed in chapter 4. The exciting field was derived from focusing the fundamental laser beam at 775 nm from a regenerative Titanium-Sapphire (Ti:Sa) amplifier system (CPA 2101; Clark MXR) onto a 3 mm thick calcium fluorite (CaF_2) crystal plate. This produced a wide band spectrum (white light continuum) extending from 340 nm to the near infrared (NIR) as shown in Figure 3.1(b). This displayed probe spectrum (Figure 3.1(b)) was measured after putting a NIR filter along its path. The beam transmitted through the sample was directed towards a spectrometer (Andor SR163) equipped with a camera (1024 pixel photodiode array, Entwicklungsbüro Stresing). The wavelength calibration of this spectrometer was always checked using a mercury-argon light source (Mikropack, CAL-2000). Good comparison of steady state and transient absorption results are achieved with using the same

setup for measurements as any noise or experimental errors emanating from the devices used will be constant in all measurements.

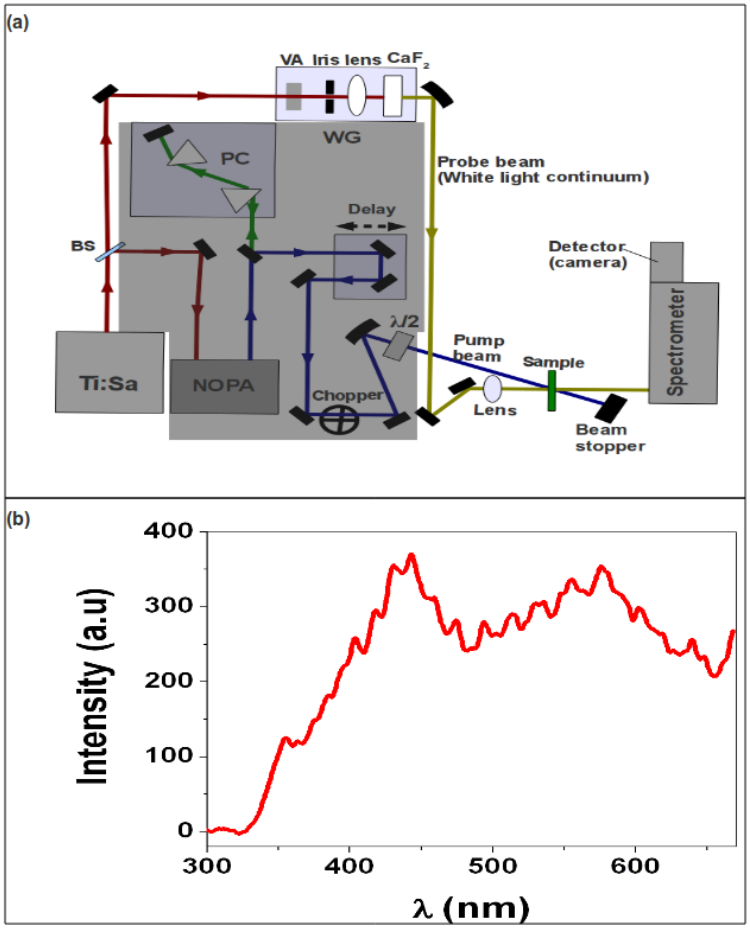

Figure 3.1: (a) The layout of the experimental set up used for performing steady state absorption measurements. The set up was the same one used for transient absorption measurements and the region covered with a transparency was not used for the current measurements. (b) The spectrum of white light continuum generated from CaF_2 crystal plate used as exciting field in steady state absorption measurements.

The obtained tetracene solution steady state absorption spectrum displayed a clear vibronic progression with spacing ΔE = 0.17 eV ($\approx$1430 cm^{-1}) in the range 390 nm to 490 nm as seen in Figure 3.2. The profiles and the position of the peaks were similar to those reported in literature [16, 31, 47, 48] indicating that the samples were identical. The obtained results have been summarized in Table 3.1. The spectrum marked the transition $S_0 \rightarrow S_1^{v=0,1,2,3}$ [16, 31, 47, 48] where v represents the vibronic bands centered at 474 nm, 444 nm, 418 nm and 395 nm. This measurement was repeated using a conventional ultraviolet - visible spectrometer (Evolution 600 UV-VIS, Thermo Scientific). The same profiles and positions of the vibrational bands were obtained thus justifying the use of our setup.

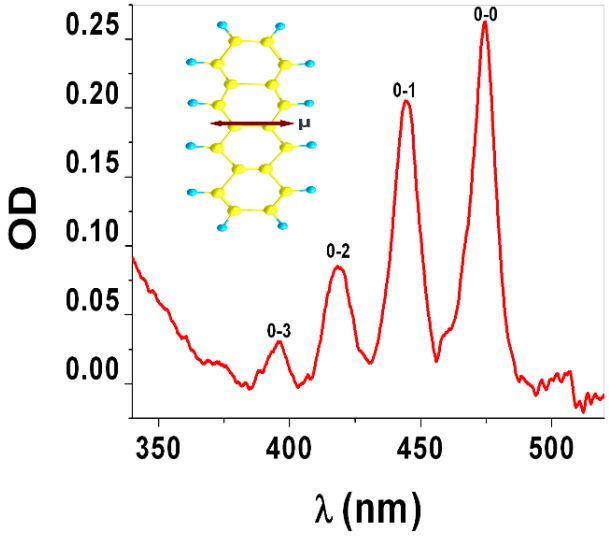

Figure 3.2: The absorption spectrum of tetracene dissolved in toluene solvent. The four peaks represent the transitions ($S_0 \rightarrow S_1^{\nu=0,1,2,3}$) where ν are the vibrational bands in S_1. The respective bands have been labeled 0-0, 0-1, 0-2 and 0-3 in the figure. OD stands for optical density (absorbance) of the sample.

Table 3.1: Table giving the experimental position of the centre of the vibrational bands in the first excited singlet state in Tc solution. The absorbance and vibrational modes (Δ E (eV)) are also given.

Transition	λ (nm)	Absorbance	ΔE (eV)
0-0	474	0.25	
0-1	444	0.20	0.18
0-2	418	0.08	0.17
0-3	395	0.03	0.17

From the lowest energy peak at 474 nm with absorbance of 0.25 in solution phase an absorption cross-section of 8.0 $\times 10^{-19}$ cm^2(molecules)$^{-1}$ was estimated (refer to Appendix A). The transition dipole moment of the measured $S_0 \rightarrow S_1$ transition is parallel to the short axis (the M axis) of the molecule as schematically shown in the inset of Figure 3.2 [14, 21, 47]. The position of the second excited singlet state $S_0 \rightarrow S_2$ was reported elsewhere to be situated at 294 nm with transition dipole moment parallel to the long axis of the molecule [31]. The peak observed below 350 nm in our sample most likely represented this latter state (S_2) and lies close to a jumble of higher energy singlet state transitions [31]. In studies done by Liu *et al* the spectra of Tc dissolved in other solvents showed no variations in shapes but with small shifts ($\approx$ 3 nm) in the positions of the peaks due to solvent shifts [47]. The absorbance values at the peaks corresponding to transitions from the ground state to the vibrational bands in S_1 ranged from 0.25 to 0.03 as given in Table 3.1.

These results showed that tetracene absorbs in a wide spectral range spanning from UV to VIS. Its absorbance is also considerably high. This makes it an interesting material to study for purposes of utilizing its properties in solar cells

and other optical devices such as light emitting diodes and transistors. It can also serve as a model system to investigate mechanisms of solar energy capture and transfer in photosynthetic light harvesting complexes. In solid state electrical devices, crystals are used. It is therefore interesting to study this same sample in crystal phase.

3.2 Single Crystals of tetracene

Now having established the energy position of $S_0 \rightarrow S_1$ transition in tetracene solution, it would be interesting to also study the influence the two molecules in the crystal unit cell will have on it. It is known from past experimental [32] and theoretical studies [16, 31, 35] that the presence of the two non-equivalent molecules in the unit cell cause energy splitting (Davydov splitting) as mentioned earlier in this work. In polycrystalline thin films, this splitting will be difficult to observe since the different orientations of the crystallites on the substrate suppresses it. Here we report on results obtained from free standing single crystals of tetracene.

The crystals were provided by Prof. Jens Pflaum of the University of Wuerzburg, Germany. They were prepared by plate sublimation under an inert gas atmosphere. Platelates of up to 5 mm lateral dimension and about 500 μm thick were obtained as shown in Figure 3.3(a). Using the results obtained from the sample in solution, one can estimate the appropriate crystal thickness for use in our measurements. To obtain an absorbance of 0.25 same as that at 474 nm in solution, one needs a crystal of thickness 920 nm (refer to Appendix A). This value showed that nanometer thick tetracene samples were required. This meant that the crystal platelates provided to us had to be cut to samples that were as thin as possible. This was achieved by means of a microtome (see Figure 3.3(b))

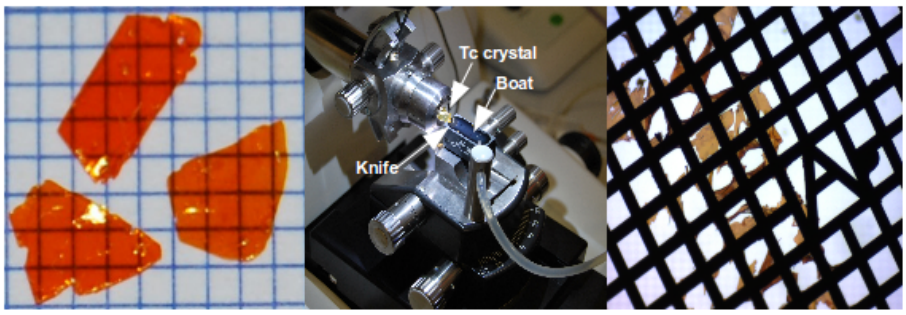

Figure 3.3: Images of (a) tetracene un-cut crystal platelates on a square grid with 1mm divisions (b) microtome and (c) a 200 nm thick Tc single crystal supported on a copper wire mesh with squares of dimensions 150 μm.

With this device, one can obtain very thin single crystals through slicing off layers of the crystal glued on a resin rod using a diamond knife. The cut pieces were let to float on water in a boat adjacent to the knife. The pieces were then fished out using a 3 mm diameter copper wire mesh with squares of dimensions 150 μm (see Figure 3.3(c)) . For this work, crystals of thicknesses 200 nm, 300 nm

and 500 nm and lateral dimensions of ≈150 μm $\times$150μm were obtained. Due to their sizes, steady state absorption measurements could not be done using conventional UV-VIS spectrometers.

Since the sizes of the crystals were so small as shown in Figure 3.3(c) , a magnifying system was necessary to align it appropriately at the sample position in the transient absorption (TA) setup. The system made in our lab for this purpose composed of a lens with adjustable position and a camera as sketched in Figure 3.4. Magnification M of the copper wire mesh supporting the crystal was

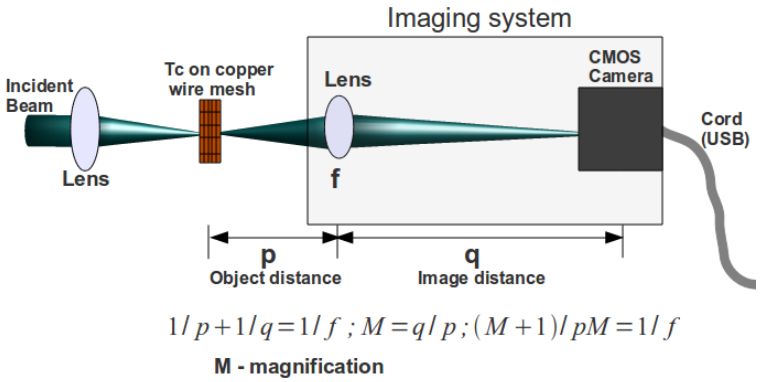

Figure 3.4: The imaging system consisting of a lens of focal length f and a CMOS camera. The camera was connected to a computer using a USB cord.

achieved through adjusting the distances p and q. For good magnification, q was made as long as possible. A maximum magnification of 3 (i.e $q/p \leq 3$) was obtainable from the system. The coordinates of the square aperture in the wire mesh containing good quality single crystal was first noted by viewing under a microscope and getting its image (see Figure 3.3(c)).

The absorbance measurements were performed at room temperature (300 K) using the same experimental setup shown in Figure 3.1(a). A Glan-Taylor calcite polarizer (providing a clean polarized field) and an achromatic half wave-plate (400 nm - 800 nm band width) for varying the polarization direction were placed along the beam. The spectrum was recorded at every 8^o additional rotation of the wave-plate. Figure 3.5 display spectra at selected polarization angles in the three crystals of thickness 200 nm, 300 nm and 500 nm.

The 0-0 vibrational peaks in the three crystals displayed existence of two components with one being suppressed at certain field polarization angles and enhanced in others. A flattening or saturation of absorbance of this same peak was noticed in the 300 nm and 500 nm thick crystals (see Figure 3.5 (b) and (c)). The two components observed at the 0-0 vibrational peaks represented transitions to the two Davydov states arising from interactions of the translationally inequivalent molecules in the unit cell as was described in chapter 2. The fact that no significant changes in absorbance was noticed with varying polarization angles in the vibrational bands higher than the 0-1 band signified that intermolecular interaction was minimum in higher excited states and maximum at vibrationally relaxed states [13] (see also Figure 3.6(c)).

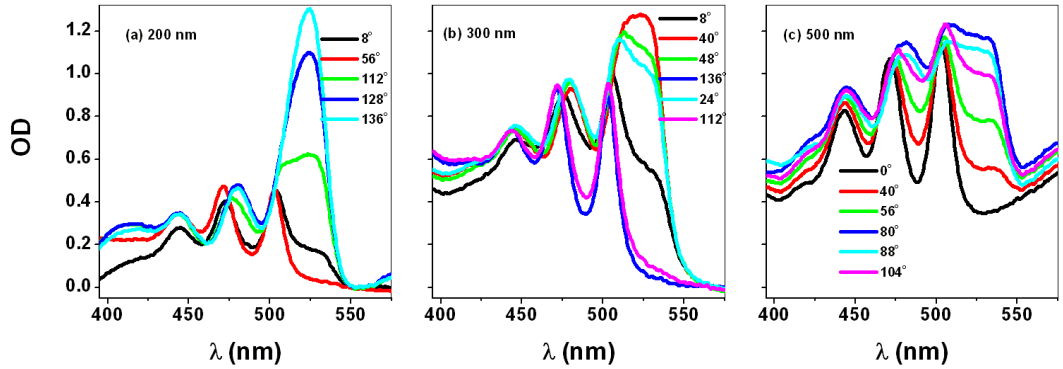

Figure 3.5: Absorption spectrum of the (a) 200 nm (b) 300 nm and (c) 500 nm thick crystals at the selected polarization angles of the incident field obtained by rotating the achromatic half wave-plate. The same OD scale in (a) applies to (b) and (c). There was a large background in the 500 nm thick crystal.

The observed saturation of absorbance at the low energy peak in the thicker crystals was attributed to increase in the number of absorbing molecules. The number of molecules excited in each of the crystals can be estimated from the excitation spot diameter (≈200 μm) and the crystal unit cell volume (583 Å^3 [13]). In the 200 nm, 300 nm and 500 nm thick crystals 2.1 $\times 10^{13}$, 3.2 $\times 10^{13}$ and 5.3 $\times 10^{13}$ molecules respectively were excited (see Appendix A). These values show clearly that there were more molecules in the thicker samples. A similar saturation of absorption with increase in crystal thickness was observed by Tavazzi *et al* in Oligothiophenes [32]. Spectra obtained through calculations done by West *et al* also displayed an increase in oscillator strength at the lowest energy bands with increase in the size of the system [21].

In order to determine the value of Davydov splitting, a number of spectra at different polarization angles were fitted with a sum of six Lorentzian functions as shown in Figure 3.6.

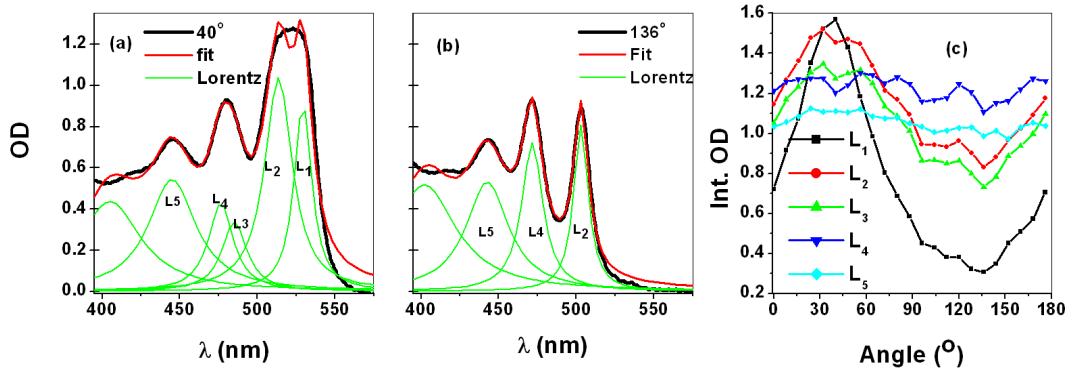

Figure 3.6: (a) and (b) Fitting of the spectra for the 300 nm thick single crystal with a sum of Lorentzian peaks. The Lorentzian peaks represented the different contributions in the respective vibrational band. (c) Variation of integrated absorbance at different polarization angles at Lorentzian peaks L_i with $i = 1, 2, 3, 4, 5$.

The 0-0 and 0-1 vibrational transition peaks were reproduced using two Lorentzians L_1, L_2 and L_3, L_4 respectively to account for the two Davydov components ob-

served in Figure 3.5 (see Figure 3.6 (a,b)). The variation of absorbance integrated over the widths of each of the Lorentzian peaks L_i with $i = 1,2,3,4,5$ at different field polarization angles are displayed in Figure 3.6(c). The high energy transitions represented by Lorentzian L_5 and L_6 (the latter not labeled) showed minimum change in absorbance with change of polarization angle implying little intermolecular interactions and therefore low Davydov splitting. L_1 represented transitions to the low energy Davydov band and it displayed a maximum and minimum absorbance at field polarization of 40^o and 136^o respectively in the 300 nm thick crystal. The fields were then thought to be respectively polarized $\parallel$ *b*- and $\perp$ *b*-axis of the *ab* crystal face [13, 14, 16, 31, 32]. It was also interesting to note that at field polarization of 40^o ($\parallel$ *b*-axis) the high and the low energy Davydov components (L_2, L_4 and L_1, L_3) were both responsible for the heights and widths of the 0-0 and 0-1 transition peaks while at 136^o ($\perp$ *b*-axis) the low energy Davydov components (L_1, L_3) were suppressed as shown in Figures 3.6(a) and (b) respectively. The suppression of one of the components at a certain field orientation signified that the projection of the transition dipole moments of the two molecules in the unit cell onto the *ab*-crystal plane were orthogonal. If this were true, then the difference between the polarization angle giving maximum and minimum absorbance at L_1 should be 90^o. A value 88^o (the average of 80^o, 96^o and 88^o angles obtained from the 200nm, 300nm and 500nm thick crystals respectively) was found. This indicated that the two polarizations were not strictly perpendicular confirming calculations done by Tavazzi *et al* where non-zero components were found in all crystallographic directions [14]. The same was also pointed out by Schlosser and Philpott as the expected result due to the triclinic crystal structure [31]. Figure 3.7 displays the spectra at $\parallel$ *b*- and $\perp$ *b*-axis field polarizations in the 200 nm, 300 nm and 500 nm thick crystals.

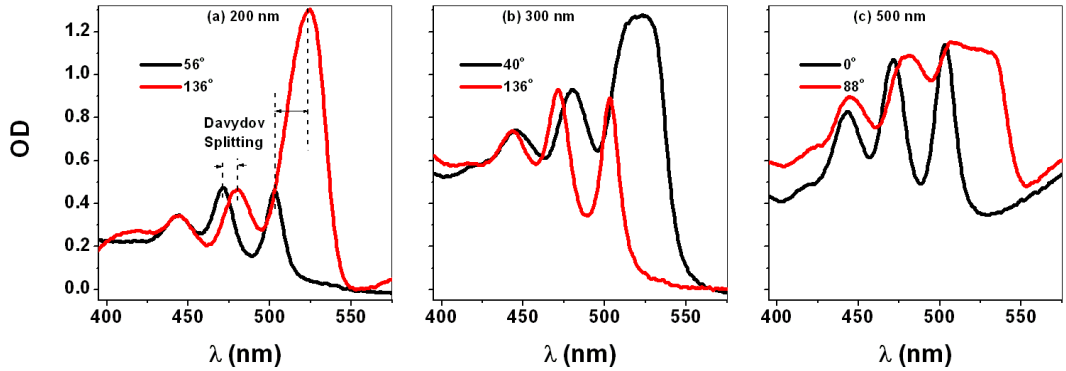

Figure 3.7: Spectrum of the (a) 200 nm (b) 300 nm and (c) 500 nm thick crystals giving the maximum and minimum absorbance representing fields polarized parallel and perpendicular to the *ab* crystal face respectively. The shift in the spectrum between the two polarizations is known as Davydov splitting.

In this work, Davydov splitting (DS) was determined in two ways. One method involved obtaining the average of centers of lorentzians L_i ($i = 1 - 5$) from spectra at different polarization angles. Splitting was then determined from $D_{00} = (E(L_2) - E(L_1))$ eV and $D_{01} = (E(L_4) - E(L_3))$ eV in the 0-0 and 0-1 band transitions respectively. From this operation, values of 0.12 eV and 0.04 eV for the two

band transitions were obtained. These were higher than the reported values of 0.08 eV [14, 16] and 0.03 eV [14] respectively but similar to what was calculated (0.11 eV) by Schlosser and Philpott using dipole approximations [31]. Table 3.2 displays the resultant averages and the estimated DS energy.

Table 3.2: Table of centre wavelengths of the Lorentzian functions, L_i ($i = 1 - 5$), used for making the fits to the spectra. These values were obtained from the average of centers at chosen angles of polarization. Spectra at eight different angles were used. D_{00} and D_{01} represented Davydov splitting.

Thickness	L_1(nm)	L_2(nm)	L_3(nm)	L_4(nm)	L_5(nm)	D_{00}(eV)	D_{01}(eV)
200 nm	528.1	503.3	480.3	472.7	443.5	0.12	0.04
300 nm	529.9	503.4	483.2	474.3	444.4	0.12	0.05
500 nm	531.9	503.3	480.5	471.7	443.6	0.13	0.05

The other method of determining DS energy which was similar to that described in literature [14, 17] was also done. It involved obtaining the difference between the centre of the 0-0 vibrational peak at minimum and at maximum absorbance of Lorentzian peak L_1 (see Figure 3.7(a)) . The spectra corresponded to those obtained with the exciting field polarized $\perp$ b- and $\parallel$ b-axis respectively. Splitting of of 0.08 eV and 0.03 eV was estimated from this method which compared well with literature values [14, 16]. Table 3.3 displays the obtained results in the three crystals.

Table 3.3: Table of experimental Davydov splitting values obtained from tetracene single crystals.

Sample	Pol.	$(0-0)$	$(0-1)$	$(0-2)$
200nm	$\perp$ b (nm)	503	472	444
	$\parallel$ b (nm)	519	477	443
	$DS_{200}(eV)$	0.08	0.03	0.01
300nm	$\perp$ b (nm)	503	474	443
	$\parallel$ b (nm)	520	480	445
	$DS_{300}(eV)$	0.08	0.03	0.01
500nm	$\perp$ b	503	472	443
	$\parallel$ b (nm)	520	477	444
	$DS_{500}(eV)$	0.08	0.03	0.01

In the two results it was found that crystal thickness had no influence on the magnitude of the splitting implying that it was a crystal specific quantity. The reasons for differing results from the two methods used was not understood. It has been known that the amount of splitting in tetracene is influenced by contributions from states higher than S_1 [31]. S_3 state for instance was shown through calculations done by Schlosser and Philpott to have a very large splitting with its low energy branch overlapping with S_1 vibrational states. The influence of this overlap was reported to depress splitting in the 0-0 vibrational band in S_1 state . Whether one of the methods used above was blind to this mixing was not exactly known. The second method, however, reproduced experimental results reported

in literature [14, 16]. Charge transfer states were also shown by Yamagata *et al* to play a role in the splitting [16].

The interaction of the excited molecules with the surrounding molecules in the ground state results in a red-shift of their energy. This shift was given by the relation $D = D^{'} - D^{0}$ in chapter 2 (see Figure 2.2). The solution to crystal shift SS provides an experimental value of this interaction. A value of 0.15 eV and 0.23 eV, 0.17 eV and 0.20 eV, and 0.17 eV in the 0-0, 0-1 and 0-2 vibrational bands (i.e $SS_{0-0,1,2}$) in the high energy and low energy Davydov states respectively were determined. The results have been given in Table 3.4. There was more shift in the low energy Davydov band ($\parallel b$) compared to the high energy Davydov band ($\perp b$) in all the crystal thicknesses.

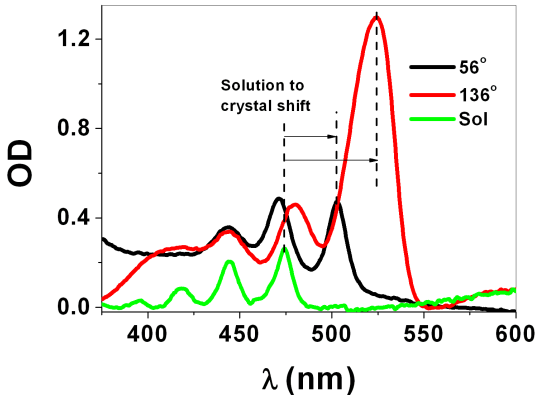

Figure 3.8: Spectra of the solution and crystal phase samples (200 nm thick crystal) plotted on the same axes showing the solvent to crystal shift.

Table 3.4: Solution to crystal shifts $SS_{0-0,1,2}$ in tetracene single crystals.

Sample	Pol.	SS_{0-0} (eV)	SS_{0-1} (eV)	SS_{0-2} (eV)
200 nm	$\perp b$	0.15	0.17	0.17
	$\parallel b$	0.23	0.19	0.17
300 nm	$\perp b$	0.15	0.18	0.17
	$\parallel b$	0.23	0.21	0.18
500 nm	$\perp b$	0.15	0.16	0.17
	$\parallel b$	0.23	0.19	0.17
Average	$\perp b$	0.15	0.17	0.17
	$\parallel b$	0.23	0.20	0.17

The positions of a number of excited states in Tc have been reported in different studies as summarized in Table 3.5 and 3.6. There is no consensus yet on the definitive positions of states higher than the first excited singlet and triplet. The presence of many overlapping singlet and triplet states in the ultraviolet and visible region of the electromagnetic spectrum made such efforts difficult.

Table 3.5: Table of the positions of the various energy states in Tc solution reported in this study and literature and the methods used for their determination. In the table Abs., Th, FP and 2-MTHF stands for absorption, theory, flash photolysis and 2-methyltetrahydrofuran respectively.

	Tc molecule / solution			
State	λ (nm)	Solvent	Method	Reference
S_1	471,441,416	Acetone	Abs	[47]
	474,444,418, 395	Toluene	Abs	our work
S_2	294	Acetone	Abs	[47]
	294		Th	[31]
S_3	274		Th	[31, 16]
T_n	485,468,440	2-MTHF	Abs	[49]
	412,385,360, 320	2-MTHF	Abs	[49]
	465	Benzene	FP	[46]

Table 3.6: Table of the positions of the various energy states in Tc crystal reported in this study and in literature and the methods used for their determination. Position of charge transfer (CT) state and the lowest energy conduction (E_c) band are also shown.

	Tc crystal			
State	λ ($\parallel b$) (nm)	λ ($\perp b$) (nm)	Method	Reference
S_1	518,477,443,419	502,471,441,416	Absorption	[14]
	520,477,444	503,472,443	Absorption	Our work
T_1	886		Fluorescence	[22]
CT	428		Electroluminiscence	[22, 29]
E_c	413		Fluorescence	[22, 50]
	400			[13]

As can be seen from tables 3.5 and 3.6 the results obtained from our samples compared well with literature values indicating that the samples were never damaged or modified during preparation. The $S_0 \rightarrow S_1$ transitions were at 474 nm, 444 nm, 418 nm, 395 nm in solution phase tetracene and 520 nm, 477 nm, 444 nm (low energy Davydov) and 503 nm, 472 nm, 443 nm (high energy Davydov) in the single crystal. The knowledge of positions of these two excitonic states will enable making informed decision on states to be interrogated in an optical measurement. The solution to crystal shift energy can also be accounted for when investigating samples in the two phases.

4. Femtosecond transient absorption spectroscopy of Tetracene

In order to successfully utilize organic semiconductors in designing new technological devices such as organic light emitting diodes (OLED), organic solar cells (OSC) and organic field-effect transistors (OFET), it is important to understand both the nature of photogenerated states and their relaxation dynamics. Such information can be obtained through performing femtosecond transient absorption spectroscopy. Here measurements done on tetracene single crystals and tetracene dissolved in toluene solvent are discussed. A number of short-lived and long-lived transient states were identified and interpreted. A brief description of the principle of transient absorption spectroscopy and of the home-built non-collinear phase-matched optical parametric amplifier (NOPA) has also been given.

4.1 The experiment

The creation and decay of excitons take place on timescales ranging from sub-100 femtoseconds (fs) to tens of picoseconds (ps) [21, 33]. In order to temporally resolve such ultrafast processes, techniques with femtosecond temporal resolution must be used. One candidate is the femtosecond transient absorption (TA) spectroscopy. This method offers the opportunity to track in real time energy and charge transfer processes, ultra-fast structural changes (isomerization) and formation of new transient species [51, 52]. Here, a fraction of molecules are promoted to an electronically excited state by means of a resonant femtosecond optical pump pulse. A second less intense pulse (the probe) then interrogates the system (molecule or crystal) at a later time τ after excitation. The probe field can either be absorbed by the excited sample (excited state absorption, ESA) or stimulate an emission (stimulated emission, SE). The entire map of transient dynamics in the sample are contained in a two-dimensional array $\triangle OD(\lambda, \tau)$ obtained from recording the spectra of the probe beam at different delay times relative to the pump pulse. This quantity represents the change in absorbance of the sample after excitation and is calculated as [51, 52]

$$\triangle OD(\lambda, \tau) = log(\frac{I_{un-pumped}(\lambda)}{I_{pumped}(\lambda, \tau)}) \tag{4.1}$$

where $I_{un-pumped}(\lambda)$ and $I_{pumped}(\lambda, \tau)$ represents the intensity of the transmitted probe beam through un-excited and excited sample respectively at a particular probe wavelength (λ) and delay τ. The transient spectra ($\triangle OD(\lambda, \tau)$) contain

contributions from various processes including ground state bleach (GSB), stimulated emission (SE) and excited state absorption (ESA) signals. The amplitudes of these transient signals at a particular time after excitation are schematically represented in the transient spectra of figure 4.1.

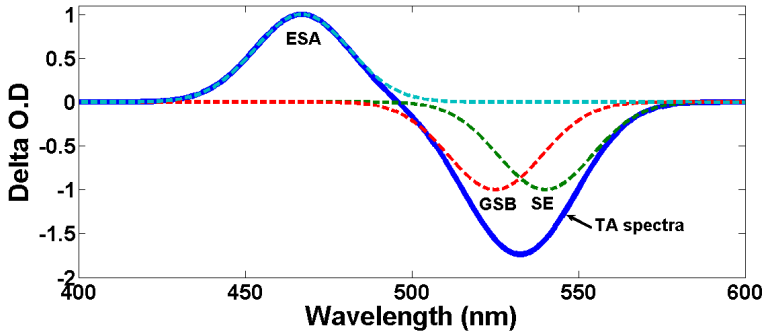

Figure 4.1: A schematic of the the TA spectra at a particular time after excitation showing the amplitudes of the GSB, SE and ESA signals. GSB and SE signals have negative amplitudes while ESA have positive. A detailed description of these signals are given in the main text of this work.

1 Ground state bleach (GSB) signals arise when the probe beam interrogates a sample electronically excited by the pump pulse. Fewer molecules will therefore be available in the ground state to absorb more energy. Consequently, the transmitted probe beam is stronger in the pumped than in the un-pumped sample. This leads to a negative peak appearing in the transient absorption spectrum $\triangle OD(\lambda, \tau)$. The persistence of such peaks indicates that not all the molecules have returned to the ground state [51, 52].

2 Stimulated emission (SE) signals appear when the probe pulse cause a de-excitation of some of the molecules to the ground state accompanied by release of photons which propagate collinearly with the probe. This leads to a more intense beam being measured through the excited than un-excited sample. They also have a negative amplitude in the transient absorption spectra but are red (Stokes) shifted with respect to the GSB signals as depicted in Figure 4.1. This is because they occur only for allowed transitions i.e those with high Frank-Condon factors (FC). The shift may sometimes be so small that both the GSB and SE signals spectrally overlap (see Figure 4.1).

3 Excited state absorption (ESA) signals are seen at wavelengths of allowed transition from populated excited states to higher-lying states through absorption of probe photons. A less intense beam will be detected at the respective wavelengths. They therefore, have positive peaks in the TA spectrum as shown in figure 4.1.

Experimental setup

The complete schematic of our experimental setup is shown in Figure 4.2. It depicts all the essential elements employed which includes the laser source, the

generation of the pump and probe beams. A brief description of each of these is given below.

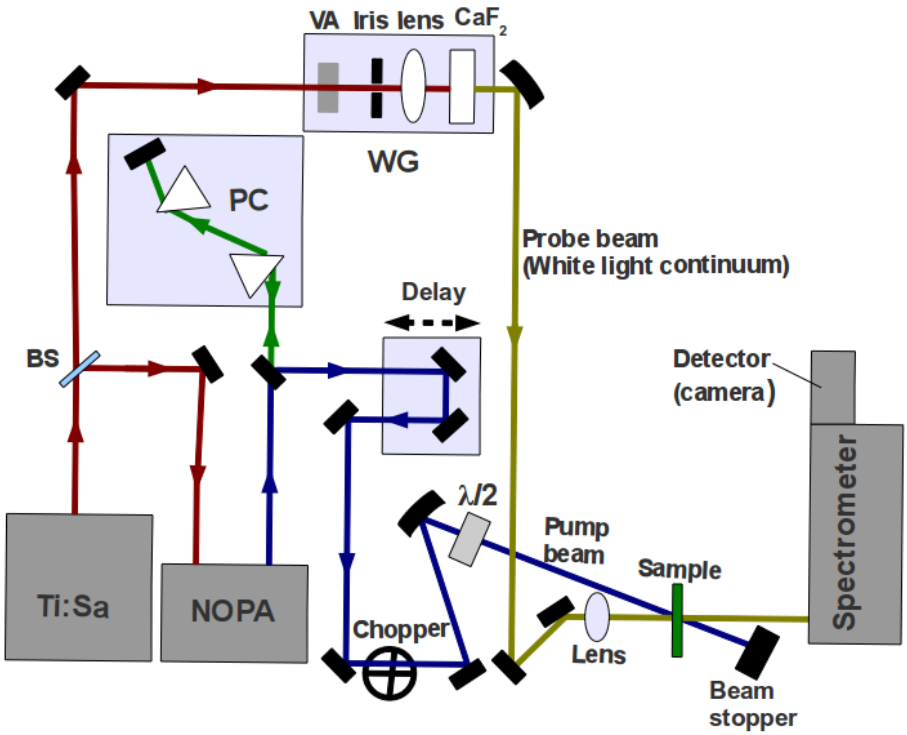

Figure 4.2: The layout of TA spectroscopy setup used in our studies. The beams in the visible regime from the NOPA are compressed using a prism compressor (PC). Part of the fundamental is used to generate white light (WG) by focusing it onto a calcium fluorite crystal plate.

The laser source

As a light source a regenerative Titanium-Sapphire (Ti:Sa) amplifier system (CPA 2101; Clark MXR) delivering pulses with an energy of 800 μJ and of $\approx$150 fs duration and centered at 775 nm was used. The pulses were produced at a repetition rate of 1 kHz.

The NOPA

The output of the Ti:Sa laser is only slightly tunable within the vicinity of 775 nm and its second harmonic at 387 nm. This limits it's use to studying only few molecules that absorb within these energy regions. A versatile spectroscopic setup that was tunable over a wide range of wavelengths was therefore required.

A powerful way to achieve this is by using a noncollinearly phase-matched parametric amplifier (NOPA). A detailed description of its operation has been done elsewhere [53, 54]. In brief, in a suitable nonlinear optical medium such as a β-barium borate (BBO) crystal, transfer of energy from a high power, fixed frequency ω_p pump beam to a lower power variable frequency ω_s signal/seed beam occur, besides, a third beam, the idler at frequency ω_i is generated such that $\omega_i < \omega_s < \omega_p$ [53, 54, 55]. This process is referred to as optical parametric

amplification/generation. In the interaction, the energy conservation

$$\hbar\omega_p = \hbar\omega_s + \hbar\omega_i, \tag{4.2}$$

and momentum conservation

$$\hbar k_p = \hbar k_s + \hbar k_i, \tag{4.3}$$

must be satisfied [54]. k_p, k_s and k_i are the wave vectors of the pump, signal and idler beams respectively. An efficient conversion is achieved when the phase matching condition

$$\triangle k = k_p - k_s - k_i = 0 \tag{4.4}$$

is met. This can be ensured through proper orientation of the birefringent crystal (BBO) [53].

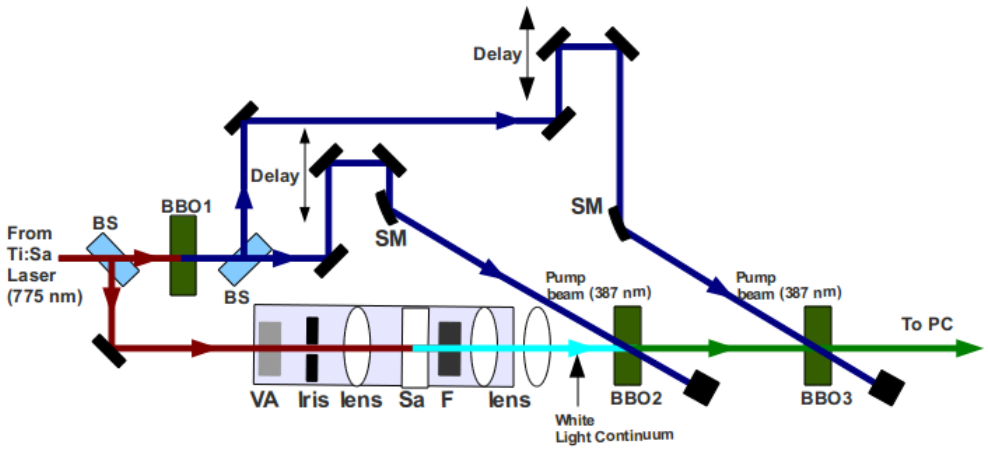

Figure 4.3: Schematic of the two-stage amplification NOPA built in our Lab. The BBO1 was used for frequency doubling of the fundamental (775 nm) while BBO2 and BBO3 were used for amplification of the desired portion of the seed pulse in a non-collinear arrangement as shown. The seed beam (VIS white light continuum) was generated by focusing the fundamental into a sapphire plate (Sa). F is a filter for the fundamental. The temporal overlap at the BBO crystal site was adjusted by manual delay stages. Spherical mirrors SM focused the pump beams into the birefringent crystals BBO2 and BBO3.

As part of this project, a two amplification stage NOPA was built which consisted of three nonlinear crystals BBO1, BBO2 and BBO3 for frequency doubling of the fundamental (FM), pre-amplification and power amplification respectively, beam splitters (BS), temporal delay stages, plane and spherical mirrors for steering and focusing respectively and white light (signal beam) generation stage as sketched in Figure 4.3. The variable attenuator (VA) and the iris in the white light generator were used to control the energy of the fundamental beam and its diameter on the sapphire crystal plate. The residual FM beam was filtered out using filter F. The three lenses were for focusing of FM into the Sapphire crystal, collimation and focusing onto BBO2 of the signal beam.

The high intensity focused into the sapphire crystal results in the production of a visible (VIS) white light continuum beam. The cause of this spectral broadening is essentially self-focusing and self-phase modulation [54, 56] although other

nonlinear effects might also contribute. The desired portion of this continuum (signal beam) is amplified in BBO2 crystal pumped by the frequency doubled FW beam (doubling done at BBO1 yielding pulses centered at 387 nm) in a non-collinear geometry as shown in Figure 4.3. Such a geometry provides a broad amplification bandwidth by broadband phase matching since the white light is linearly chirped i.e some frequencies are in-front and some are at the tail of the pulse as it travels [53]. Phase-matching bandwidth can be increased further by adjusting the orientation of the BBO crystal. From this, spectrally broad pulses are produced which can support shorter pulses. It is known that in linear arrangement, the faster propagating idler generates more signal beam and at the same time the slower signal also generates more idler as they travel in the crystal leading to temporally broadened pulses [53]. BBO3 is used for further amplification in the NOPA.

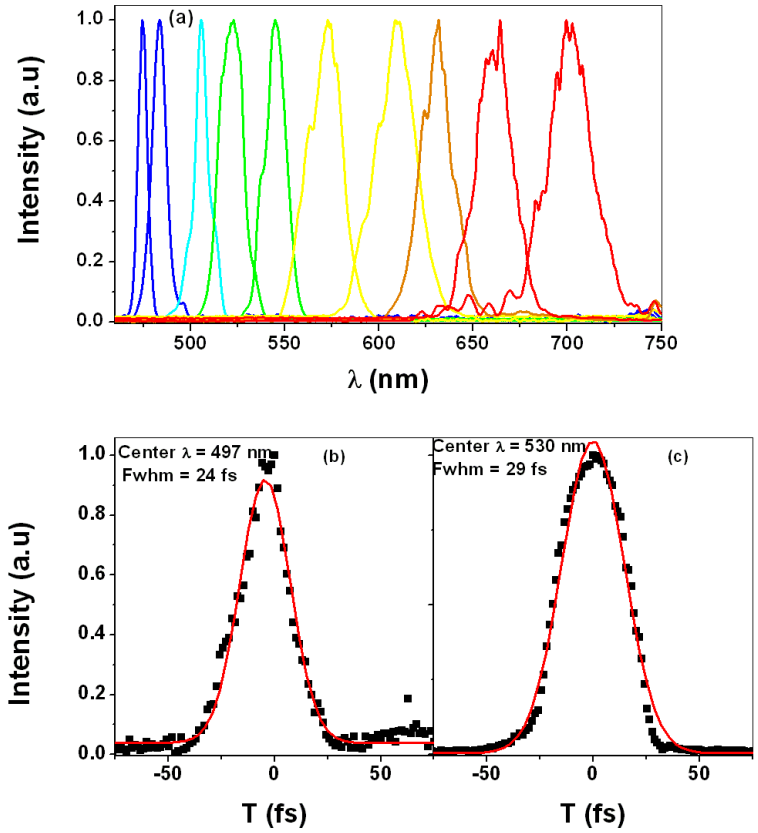

Figure 4.4: (a)The NOPA spectrum. This serves to show the spectral tunability range of the system which extends from 450 nm to 700 nm. The autocorrelation traces of the compressed NOPA output pulses centered at (b) 497 nm and (c) 530 nm are also shown. Pulses as short as 24 fs were obtained.

Figure 4.4(a) shows the spectrum of the NOPA which spans from 450 nm to 700 nm. This showed that the experimental setup can now be tuned spectrally with ease within this band. The chirped VIS pulses outputting from the NOPA were compressed further by using a pair of Brewster angle fussed silica prisms as shown in Figure 4.2. From this system, pulses as short as 24 fs (fwhm) shorter

than the duration of the pump pulse (≈150 fs) as measured using a home-built D-mirror autocorrelator were obtained as shown in Figure 4.4(b) and (c)

The pump beam

In our TA studies, two separate experiments were done. In one, the sample was pumped at 387 nm and in the other done at 530 nm. The former was obtained from steering the beam derived from BBO1 in the NOPA (see Figure 4.3) to the sample position via a retro-reflector mounted on a computer controlled linear delay stage, a beam chopper and a half wave-plate in that order as shown in Figure 4.2. The chopper wheel operated at 500 Hz blocked every second pump pulse leading to alternating pumping and no pumping of the sample. Changes in the optical density $\triangle OD$ were then possible to calculate. The wave-plate was for varying the beam polarization.

For VIS excitation (at 530 nm), the NOPA was tuned such that the appropriate portion of the seed beam was amplified. The chirped NOPA output pulses with energies upto 30 μJ were then compressed using a sequence of two Brewster prisms to about 30 fs full-width at half maximum duration as was measured with a D-mirror autocorrelator (not shown in Figure 4.2). Details of the auto-correlator can be found in [57]. The resultant beam was then steered to the sample for pumping as was described above.

The probe beam

Most organic molecules have absorption bands in or extending into the UV spectral region of the electromagnetic (EM) spectrum. Examples include anthracene and tetracene. It is therefore useful to have probe pulses covering ultra-broad spectral range at once. This enables simultaneous probing of a large percentage of the transient species generated by the action of the pump pulse. In our set up, this was achieved by focusing about 1 μJ of the original laser beam onto a 3 mm thick calcium fluorite (CaF_2) crystal plate. This resulted in the generation of a continuum extending from 340 nm to the near infrared shown in Figure 3.1(b).

The variable attenuator (VA) and the iris in the white light generator (WG) (see Figure 4.2) were used to control the energy and numerical aperture of the fundamental beam and its diameter on the CaF_2 crystal. This ensures generation of a stable and good quality (i.e one filament) white light. The crystal was mounted on a motor moving in a circular motion to reduce chances of damage. The resulting probe beam after passing through the sample was then dispersed in a spectrometer (Andor SR163) equipped with a camera (1024 pixel photodiode array, Entwicklungsbüro Stresing) as shown in Figure 4.2.

Chirp correction

The white light continuum probe beam was linearly chirped. Due to this, the temporal overlap of the pump and probe pulse (i.e time zero) was wavelength dependent as shown in Figure 4.5.

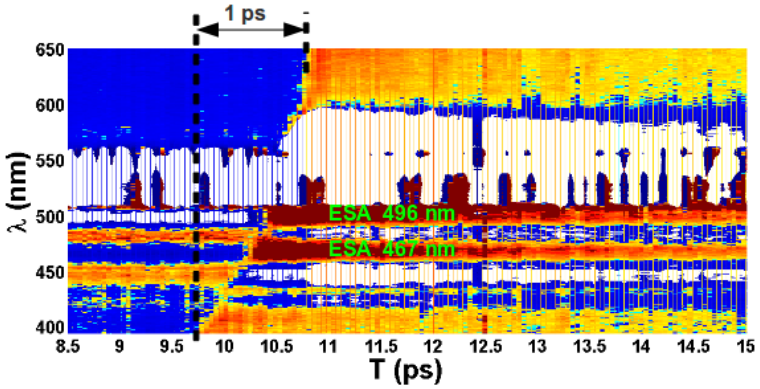

Figure 4.5: The chirp of white light continuum as seen in the raw transient absorption spectrum of 300 nm thick tetracene single crystal excited at 530 nm. The short wavelengths (400 nm) were ahead of the long wavelengths (650 nm) by approximately 1 ps.

This resulted in ≈1 ps temporal dispersion between 400 nm and 650 nm. The raw data had to be corrected for this chirp in order to obtain the transient spectrum at a particular time. This was done by fitting about 5 time zero points at selected wavelengths with a low order polynomial to interpolate time zero over the whole data set. The transient spectra reconstructed after this interpolation along the time axis contained all the molecular dynamics of interest.

For our studies, the pump beam's diameter (≈ 300 μm) on the sample was larger than that of the probe (≈ 150 μm) to ensure that only the pumped region was always probed. This was checked by imaging a wire mesh placed at the sample position and with squares of known dimensions onto a camera connected to a computer. During the experiment the average of between 1500 and 2000 spectra were recorded at every τ probe delay. Excitation power of 120 μW and beam spot diameter of 200 μm on the sample was used in all the experiments unless otherwise stated. The polarization of the probe beam with respect to the *b*-axis of the *ab* crystal face was adjusted using an achromatic wave-plate (400 - 800 nm). For tetracene in toluene, excitation was done at a magic angle of 54.7^o in order to eliminate effects due to the re-orientation of the transition dipole moments.

4.2 Transient absorption spectroscopy of Tetracene solution

A good characterization of the properties of a sample can be achieved through studying it in all the possible phases (gas, liquid and crystal). The ideal case is studying an isolated molecule (i.e in gas phase). However, many ultra-fast laser spectroscopy setups are not designed for gas phase systems. The normal practice has been to dissolve the sample of interest in a suitable solvent resulting in molecules that are separated by a large distance in comparison to those in the crystal. The behavior exhibited by this system was then assumed to be similar to that of an isolated molecule (monomer). Here, Tc was dissolved in toluene solvent

obtaining a concentration of 3.1 $\times 10^{18}$ molecules/cm^3. This was the same sample used for steady state absorption measurements described in chapter 3.

The purpose of this study, as pointed out earlier, was to identify transient species and their decay life times in the monomer and use the obtained results in making comparison with those of the crystal. This will enable study of effect of orderly aggregation of the molecules in the crystal on the monomer energy levels.

The sample was pumped at 387 nm at room temperature and probed with white light continuum . The idea was to excite higher states and then probe the temporal evolution of the system. This pumping accessed states overlapping the 0-3 (395 nm) and 0-4 (374 nm) vibrational bands in the $S_0 \rightarrow S_1$ transition (see Table 3.1 in chapter 3). The transient absorption spectrum obtained was represented in a two-dimensional (2D) array $\triangle OD(\lambda, \tau)$ shown in Figure 4.6(a). This spectrum contained all the relevant accessible information on the transient dynamics in the excited (pumped) sample. It displayed them in terms of change in absorbance as a function of excitation wavelength (λ) and probe pulse delay (τ). Slices of this spectrum along the time axis at a given wavelength provided transient decay kinetic traces while slicing along the wavelength axis at a given probe delay gave transient spectra traces like those shown in Figure 4.6(b). The

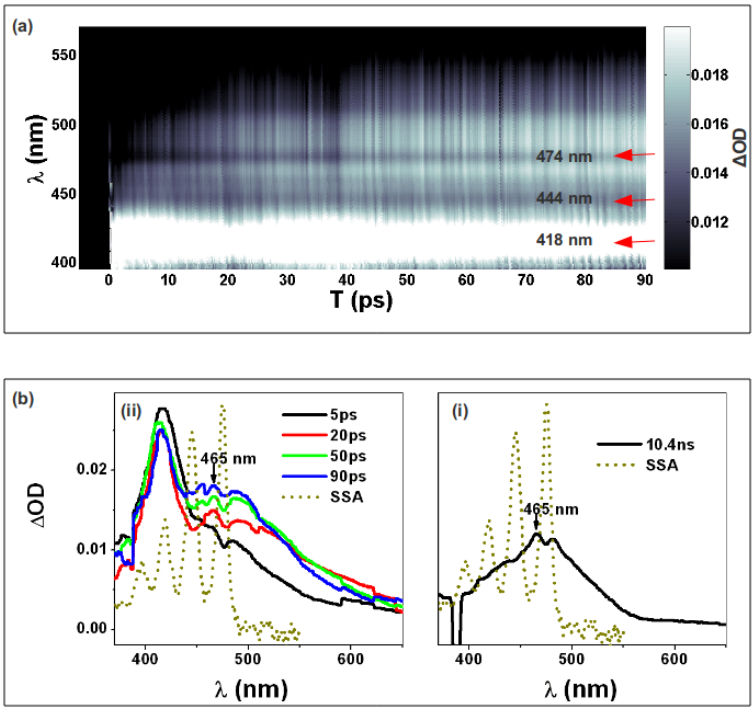

Figure 4.6: (a) 2D TA spectrum with GSB signals at 444 nm and 474 nm indicated together with the intense positive signal at 418 nm. (b) The traces obtained from slicing the 2D spectrum along the wavelength axis at a given time plotted together with a rescaled steady state absorption (SSA) spectrum plotted on the same axes so as to identify GSB signals. These signals appeared as small minima on the TA traces.

obtained TA spectrum displayed only a positive signal with a brighter band at approximately 418 nm and bands of minimum intensity at approximately 474 nm and 444 nm (see Figure 4.6(a)). Slices taken along the wavelength axis at given probe delays revealed these features clearly as shown in Figure 4.6(b). The less

bright (minima) bands in the 2D spectra appeared as dips in the traces and represented GSB signals as elucidated by plotting a rescaled steady state absorption spectrum on the same axis. These were in fact negative signals superimposed on top of a positive ESA signal.

The positive TA signal that was detected indicated that excited state absorption (ESA) plays a big role. The traces also show an increasing amplitude with time at the 444 nm to 550 nm region of the peak accompanied by a decrease at around 418 nm (see Figure 4.6(b)(i)). This behavior signified transfer of excitation energy from higher-lying states (vibrational or electronic) to the lower ones. This transfer was complete by 10.4 ns as by this time the 418 nm peak was no longer prominent compared to that around (444-550) nm as shown in Figure 4.6(b)(ii) .

The other notable feature in the transient spectra was the small maximum on the positive signal at 465 nm situated on top of the region of the minimum between the $0-0$ and $0-1$ vibrational bands in the $S_0 \rightarrow S_1$ transition as shown in Figure 4.6(b). A decay kinetic trace taken at around this ESA feature displayed a steady rise as shown in Figure 4.7. As mentioned, ESA signal was responsible for the positive signal observed but it was difficult to isolate the trace of the small maximum from those that overlaps with it. For this reason, no attempt was made to fit an exponential function to extract the time constant as it would be hard to make a definitive attribution of the dynamic responsible.

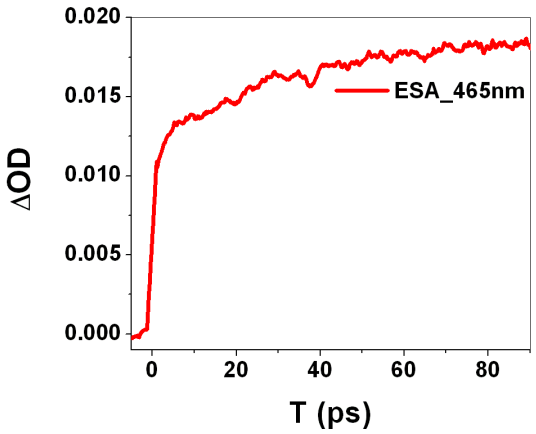

Figure 4.7: The decay kinetic trace of ESA signal at 465 nm in Tc dissolved in toluene.

The feature was more pronounced in the 10.4 ns spectra indicating its long live nature (see Figure 4.6(b)(ii)). About 38 % of excited singlet states are expected to have decayed by this time since their decay lifetime in Tc dissolved in benzene is reported as 23 ns [26]. A state situated at 468 nm was previously attributed to excited triplet - triplet absorption in studies done by Pavlopoulos on Tc dissolved in 2-methyltetrahydrofuran (2-MTHF) [49]. The same excited triplet transition was noted at 465 nm in Tc dissolved in benzene by Bensasson and Land [46]. We can therefore assign the observed feature at 465 nm to $T_1 \rightarrow T_n$ transitions.

The appearance of this feature (the small maximum at 465 nm) assigned to $T_1 \rightarrow T_n$ transitions in solution by 20 ps after excitation was puzzling. This was because population of triplet states usually happens via inter-system crossing which involves spin inversion and therefore proceeds slowly (nanoseconds to

microseconds) [20, 39]. The first probable explanation was that there was dimerization or aggregation of Tc molecules in toluene solvent which then facilitate, due to their closeness, the formation of triplet states in sub-nanoseconds timescale through singlet exciton fission just the same as it happens in polycrystalline thin films [1, 23] and single crystals [33]. If this were so, then an additional red-shifted peak attributed to dimers would be seen near the 0-0 vibrational band in the steady state absorption spectrum. Clearly, the steady state spectrum displayed in Figures 3.2 and 4.6 did not show any additional low energy peak near the 0-0 vibrational band. This rules out dimerization or aggregation as responsible for the fast production of triplets. The only logical explanation was that ultra-fast intersystem crossing occur. This can happen when the first excited singlet state was either at a higher energy or degenerate with the second (T_2) or higher excited triplet (T_n) states as sketched in Figure 4.8. This then provides the populated excited singlet (S_1 or S_n) states with an additional relaxation channel through excited triplet states.

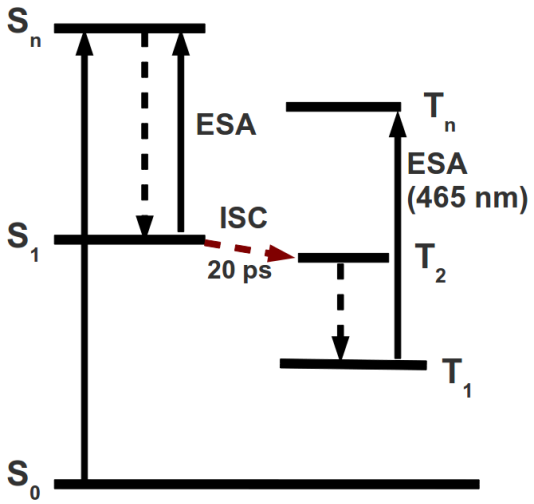

Figure 4.8: A schematic of the energy level diagram of Tc dissolved in toluene. The second excited triplet state (T_2) was thought to be situated energetically lower than S_1 and so making ISC a probable relaxation channel and proceeding on 20 ps timescale. ESA signals which were responsible for the observed broad positive peak were sketched as emanating from both the triplet and singlet states.

4.3 Transient absorption spectroscopy of Tetracene single crystals

As mentioned before, the high optical density of tetracene crystals meant that very thin crystals are required for performing transmission measurements of which transient absorption spectroscopy is one of them. This explains why few reports on ultra-fast dynamics in tetracene single crystals are available in literature. Most such studies are on polycrystalline thin films [1, 23] and the author of this work came across only one on Tc single crystals with transient changes in reflectivity performed [33]. The disadvantage of the latter approach is that only the surface and first few layers of the crystal is probed and not the volume. In polycrystalline

thin films on the other hand, due to the different orientation of Tc molecules on the substrate surface, signatures of $T_1 \rightarrow T_n$ transitions may be difficult to identify in TA spectroscopy as they will be weak and would be buried under the experimental noise [23]. In this work, free standing single crystals of thicknesses 200 nm and 300 nm were cut from the provided platelets using microtome as described in chapter 3.

It is expected that the feature assigned to $T_1 \rightarrow T_n$ transitions in Tc solution become prominent in the crystal due to the high density of molecules. It has also been established that the preferred relaxation channel of excited singlet states in Tc is through the formation of triplet states [1, 33, 39, 41, 42]. With ultra-fast transient absorption measurements, different photogenerated transient states in the crystal can be identified and their interactions and temporal evolution studied. Some of these include observation of transitions associated with higher excited singlets and triplets. These transitions are expected to be polarized due to the different orientations of the dipole moments of the two molecules in the unit cell (Davydov splitting) as discussed in chapters 2 and 3. This can be elucidated by studying the transient spectra obtained with the probe beam polarized $\parallel b$ and $\perp b$. The subsequent sections that follows explores these dynamics in the two crystals of different thicknesses.

TA spectroscopy of a 300 nm thick Tc single crystal excited at 387 nm and probed with beam polarized $\parallel b$-axis

The transient absorption spectrum of the 300 nm thick crystal obtained after exciting (pumping) it at 387 nm and with probe beam polarized $\parallel b$ of the ab plane revealed a number of negative and positive peaks as shown in Figure 4.9. This signified the existence of both ground state bleach (GSB) or stimulated emission (SE) and excited state absorption (ESA) signals respectively. The positive peaks were centered at 467 nm, 498 nm and 540 nm while the negative peaks were centered at 447 nm, 482 nm and at 540 nm as shown in Figures 4.9(a) and 4.9(b). The 2D spectrum (4.9(a)) display the positive signals as bright bands and negative ones as dark/black bands. These features become more evident in the traces obtained from slicing the 2D spectrum along the wavelength axis at a given time after excitation as shown in Figure 4.9(b).

Deconvolution of this complicated spectrum was done in two ways. One way involved plotting both TA and rescaled steady state absorption (SSA) spectrum in the same axes. In the other, a reconstruction of the TA trace at a given time was done using a fit generated from sum of Gauss functions centered at different positions on the spectrum. These two methods are discussed below.

As has been pointed out, GSB signals have negative amplitudes in the TA spectrum. They are seen at positions corresponding directly to SSA bands. Figure 4.10(a) consisting of a rescaled SSA spectrum and that of TA confirms this point. The negative peaks centered at 447 nm and 482 nm were consequently attributed to GSB signals. It was also noted that the GSB peak at 520 nm was suppressed due to high optical density at this region for the present crystal thickness. Summing the two spectra (TA and rescaled SSA spectrum) should result in only peaks associated with the positive ESA and the negative SE signals remaining as

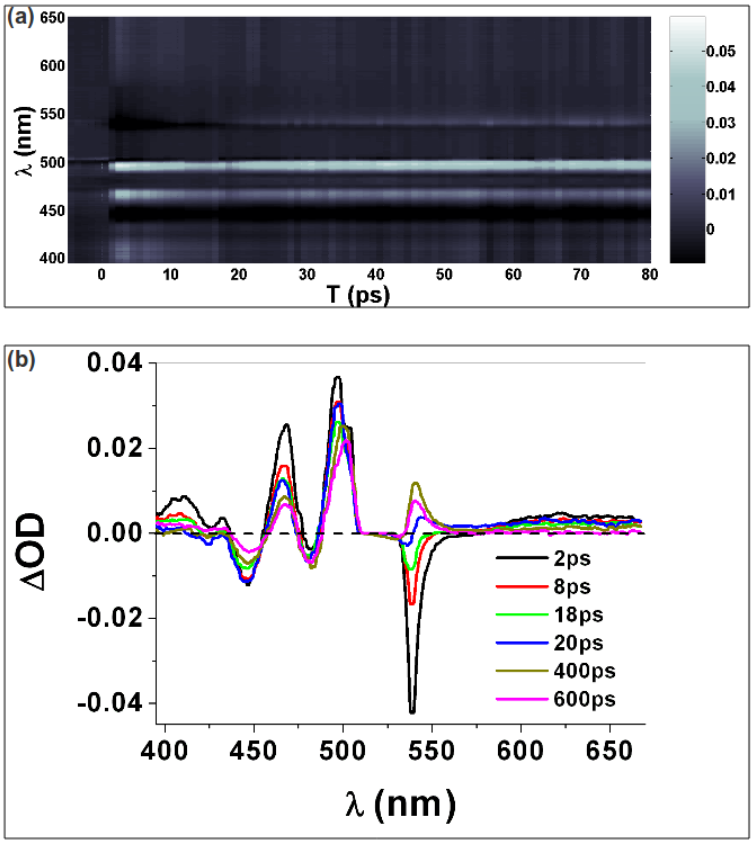

Figure 4.9: Transient spectra for the 300 nm thick crystals pumped at 387 nm showing (a) two-dimensional spectra with the white/bright bands representing increased absorption, excited state absorption (ESA) while the dark/black bands represents either ground state bleach (GSB) or stimulated emission (SE). Slices along the wavelength axis at specific times gives the transient spectra represented on (b).

shown in Figure 4.10(b). Peaks at around 467 nm and 498 nm were therefore attributed to ESA signals while the negative peak at around 538 nm was assigned to SE signals.

The deconvolution method employed above served only to identify GSB, SE and ESA signals based on their amplitudes and positions relative to the SSA spectrum. Given that within the spectral region (UV-VIS) of our study, ESA and GSB signals in Tc spectrally overlap a more rigorous method was required. A sum of Gauss functions were used to generate a fit to the transient spectra at preferably early time, say 1 ps, after excitation so as to capture a significant percentage of dynamics as shown in Figure 4.11. The Gauss functions used were of the form

$$G = A * exp[-4\pi log2((\lambda - \lambda_0)/\sigma)^2] \tag{4.5}$$

where A, λ, λ_0 and σ represented the amplitude, the wavelength, center wavelength and the full-width at half maximum (fwhm) respectively. The fit parameters were as given in table 4.1. The Gaussians at different positions were grouped basing on the earlier assignments on the contributions of the respective peaks i.e GSB, ESA and SE signals.

The positions, apart from the amplitudes, of the Gaussian peaks did not change significantly over the temporal scan range of our experimental set up. As can be

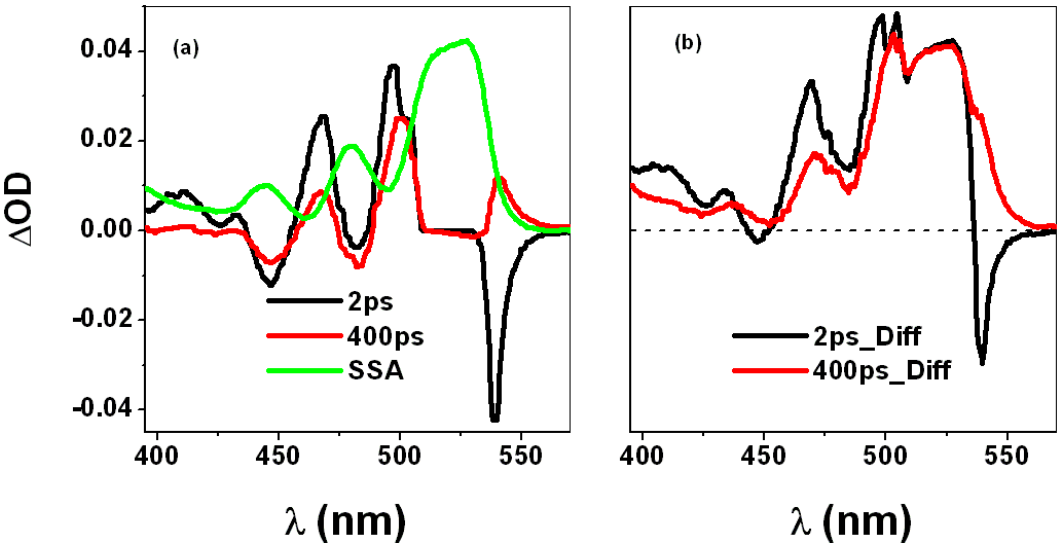

Figure 4.10: Transient spectra at 2 ps and at 400 ps after excitation plotted together with a rescaled steady state absorption (SSA) spectrum is shown in (a). The negative peaks were at the positions of the $0-1$ (peak at 482 nm) and $0-2$ (peak at 447 nm) vibrational band transitions in S_1 state. The $0-0$ (at around 525 nm) vibrational transition was suppressed. In (b) the spectra after adding the rescaled SSA spectrum to the transient absorption spectrum.

Table 4.1: The parameters used for the sum of Gauss functions fit used in Figure 4.11 for the 300 nm thick crystal. The Gaussians were grouped into GSB, ESA and SE based on their positions and the assignments made above on the contributing signals.

	GSB			ESA			SE		
Gaussian	G1	G2	G4	G3	G5	G6	G7	G8	G9
λ_0 (nm)	443	449	480	467	496	502	538	538	544
σ (nm)	7	10	9	14	11	6	6	2	11
A (a.u)	-0.009	-0.018	-0.016	0.008	0.022	0.012	-0.027	-0.010	-0.016

seen in Figure 4.11 the fit reproduced the general profile of the transient spectra. The Gaussian peaks at the respective positions (see Figure 4.11) represented transitions contributing to the observed transient absorption peak. The descriptions of each of the signals are given in the paragraphs that follows.

ESA signals (G3, G5, G6)

These are usually positive signals resulting from absorption of the probe pulse photons by molecules already promoted to excited states by the pump pulse. The excited states can either be singlets or triplets. The latter are characterized by longer decay times extending into milliseconds time scale (0.2 ms has been reported for Tc crystals [30]) compared to the former which decay within the picoseconds timescale at room temperature (300 ps for Tc crystals has been reported [25]). This property can be used in distinguishing between singlet and triplet excitons.

In our crystals the positive peaks were fitted with Gaussians G3, G5 and G6 centered at 467 nm, 496 nm and 502 nm respectively as shown in Figure 4.11. G5 and G6 reproduced the same TA peak. Obtaining kinetic decay traces around

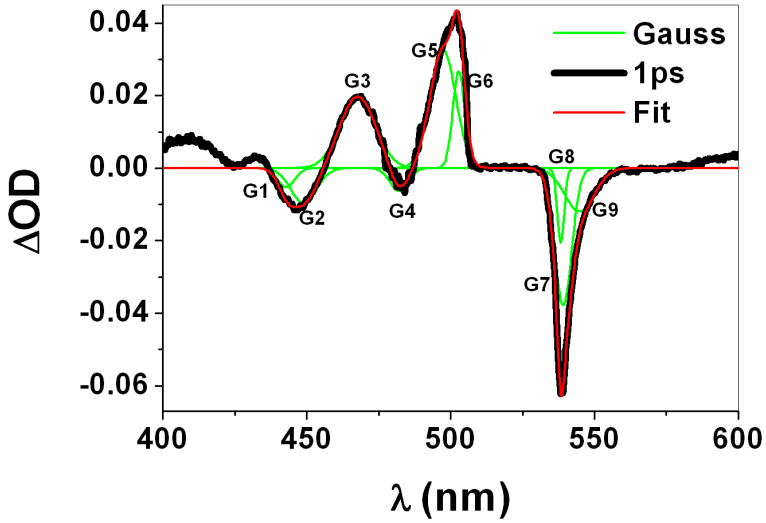

Figure 4.11: A sum of Gaussian functions fitted on the transient spectrum at 1 ps showing that it reproduces well its general profile. The positions of the Gaussian peaks used in creating the fit are also shown.

these regions will help in identifying the dynamics causing them. This was done by slicing the 2D spectrum along the time axis at the center wavelength (λ_0) and integrating the changes in absorbance ($\triangle$OD) over the widths (σ) of the respective Gaussians (see table 4.1). This resulted in the traces given in figure 4.12.

These traces revealed dynamics occurring in four time regions. The first one involved a sub-picoseconds rise as shown in figure 4.12(a). This was then followed by a decay with a time constant of 6 ps (an average of 6, 8 and 5 in Table 4.2) obtained from applying a single exponential fit of the form

$$F(t) = \mathrm{y}_0 + A \times \exp(\frac{-t}{\tau}) \tag{4.6}$$

where y_0, A and τ represented the offset, the amplitude and the decay time constant respectively. The fitted data of two of the ESA signals' traces are shown in Figure 4.13 and the obtained decay time constants are given in table 4.2.

Table 4.2: Table of decay time constants for the ESA signals represented in Figure 4.12 for the 300 nm thick crystal.

	ESA		
Gaussian	G3	G5	G6
λ_0 (nm)	467	496	502
τ (ps)	6	8	5

The third time region involved a subsequent rise at about 50 ps after excitation. The latter dynamics, after equilibrating, displayed a decay extending beyond 2.6 ns in G3 (467 nm) and G5 (496 nm) as shown in Figure 4.12(b) and (c) respectively. Oscillations on the traces were also noticed.

The long live decay dynamics observed at G3 (467 nm) and G5 (496 nm) as shown in Figure 4.12(b) and (c) can be attributed to absorption by molecules in

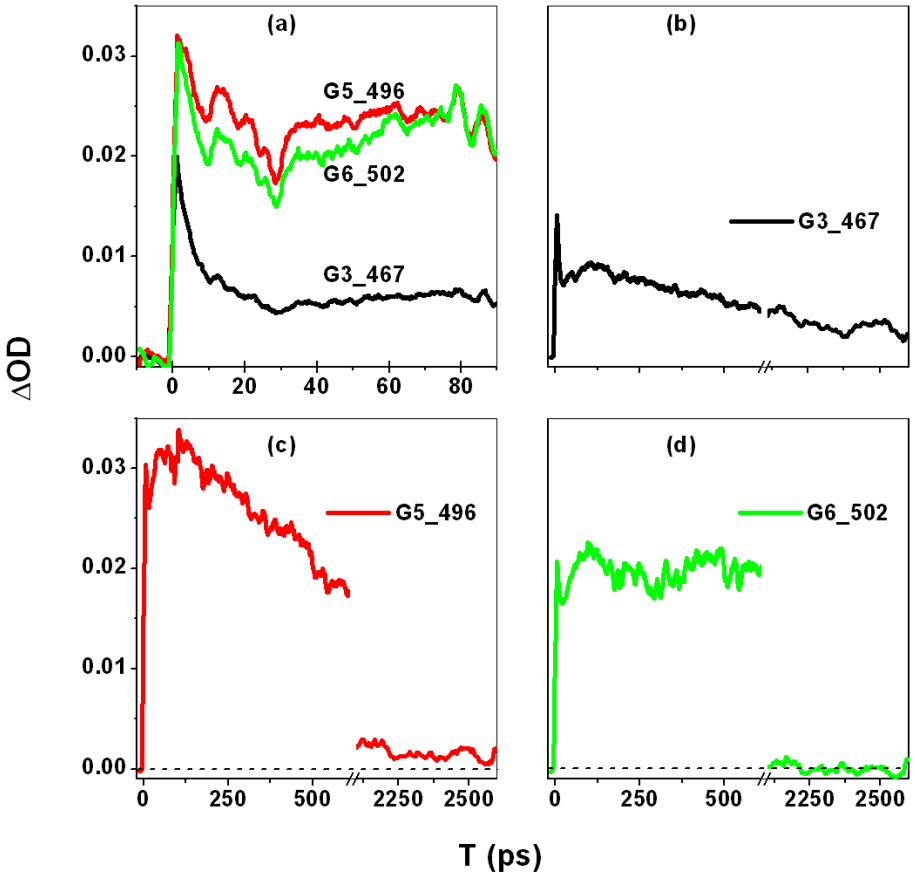

Figure 4.12: The decay kinetic traces of ESA signals G3 (467 nm), G5 (496 nm) and G6 (502 nm) with (a) showing the initial decay (b) and (c) a decay extending beyond 2.6 ns at 467 nm and 496 nm respecively and (d) showing that G6 is decayed by 2.6 ns.

the T_1 state. This was supported by the fact that G3 was close to 465 nm where a similar transition was identified in solution phase tetracene in this work and also in reference [46]. The attribution of the latter peak (G5 at 496 nm) was based on a similar assignment made by Grumstrup *et al* on transient absorption studies on polycrystalline Tc thin films [1]. Dynamics represented by G6 (502 nm) were thought to be due to trapped excitons at crystal defect sites. The most common structural defects in molecular crystals are dislocation planes where a part of the crystal is displaced relative to its neighborhood [13]. They are known to act as traps for excitons and charge carriers.

Triplet excitons in our crystals are thought to be formed rapidly at sub-ps timescales. This is possible through direct fission of higher excited singlet states (S_n states pumped at 387 nm) via the multi-exciton (ME) state ($^1(T_1T_1)$) to form triplets ($S_n \rightarrow 2T_1$) as schematically depicted in Figure 4.14. A similar fission occurring on 300 fs timescale was reported recently by Thorsmoelle *et al* on Tc single crystals pumped at 400 nm [33]. The resulting triplets explains the persistence of G3 (467 nm) and G5 (496 nm) after the initial decay. The subsequent rise observed at about 50 ps after excitation most likely represented the onset of the thermally activated ($\triangle E$) singlet fission i.e $S_1 \rightarrow 2T_1$ (see Figure 4.14). The large amplitudes and cross-sectional areas of these positive signals signified that exciton fission was the dominant relaxation channel in tetracene. A discussion on

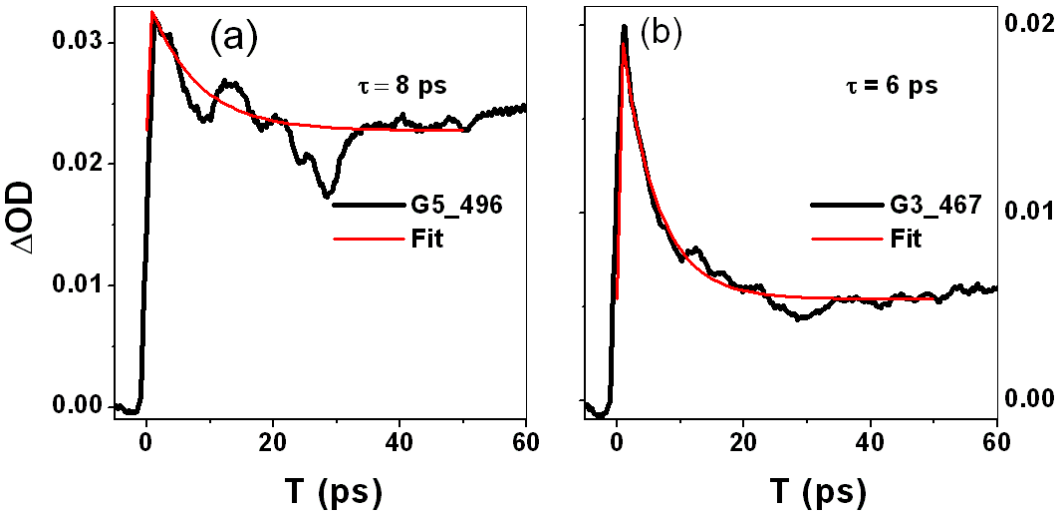

Figure 4.13: The initial rapid decay dynamics fit with a single exponential function for transition represented by (i) G5 (496 nm) and (ii) G3 (467 nm). Time constants ranging from 5 ps to 8 ps as seen in Table 4.2 were obtained.

this will be given in sections that follows.

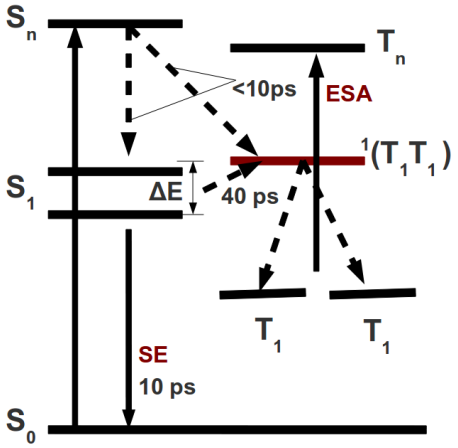

Figure 4.14: A schematic showing the states involved in exciton fission with the two Davydov states, high energy and low energy, in S_1 shown. The high energy Davydov state is close to the multi exciton (ME) state $^1(T_1T_1)$. Exciton fission occurs through two channels, one from $S_n \rightarrow ^1(T_1T_1)$ occurring in sub-10 ps timescale and the other through a thermally activated ($\triangle E$) first excited singlet exciton fission $S_1 \rightarrow ^1(T_1T_1)$ occurring on 40 ps timescale. The two coupled triplet excitons in the ME (or optically dark) state then diffuse apart resulting in two triplet excitons localized on individual molecules. The observed ESA signal was then the $T_1 \rightarrow T_n$ transition. Stimulated emission (SE) occurs from the vibrationally relaxed first excited state, here thought to be the low energy Davydov state, on 10 ps timescale.

The initial decay observed in these signals with 5 - 8 ps time constants can be attributed to either overlapping $S_1 \rightarrow S_n$ and $T_1 \rightarrow T_n$ transitions or to exciton-exciton annihilation. Overlap of excited singlet and triplet transitions are known to occur within the UV and VIS spectral regime in Tc. This has always resulted in complicated transient absorption spectra as was also seen in

solution phase sample. The rate of this decay was found to increase with increase in excitation power as shown in Figure 4.15. The decay timescale changed from 4 ps to 2 ps upon increase in excitation power from 170 μW to 290 μW respectively. The time constants were extracted from applying fit of the form $y(t) = G(t) \otimes [\theta(t)\{y_0 + A_1\, exp(-t/\tau)]$ where $G(t)$, $\theta(t)$, y_0, A_i, τ represented the Gaussian instrument response function, a step function, offset, amplitude and time constants respectively. It is known that high excitation strengths increases

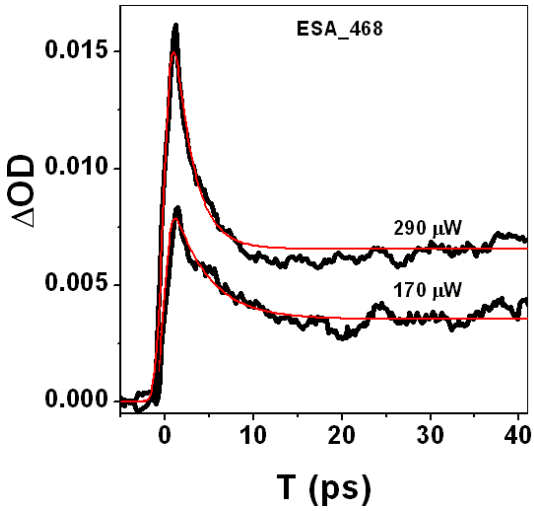

Figure 4.15: The influence of increase in excitation power on the initial decay of ESA signal at 468 nm in the 300 nm thick crystal. The decay time constant changed from 4 ps to 2 ps with increase in excitation beam power from 170 μW to 290 μW respectively. The amplitudes were also seen to increase.

the probability of exciton-exciton annihilation occurring [13] in molecular crystals as was mentioned in chapter 2. The result in Figure 4.15 served to show that exciton-exciton annihilation was one of the contributors to this decay. A similar attribution was recently made by Burdett *et al* in studies done on polycrystalline thin films by [24].

The oscillations observed in the kinetic traces (see Figures 4.12(a) and 4.15) were independent of excitation power (pulse fluence) indicating that they emanated from dynamics in the crystal. Burdett *et al* attributed them to acoustic modes excited by sudden heat input from rapid exciton-exciton annihilation [24]. They also recently explained similar oscillations seen in delayed fluorescence decays of solution-grown Tc single crystals as being caused by coherent superposition of the states in the triplet pair state $^1(T_1T_1)$ [58]. It should be recalled that this optically inaccessible state is a triplet state with a singlet character and its purpose is to mediate singlet fision.

GSB signals (G1, G2, G4)

These negative signals reflect de-population or bleach of the ground state. They represent positions where $S_0 \rightarrow S_1^v$ transitions occurred through the action of the pump pulse ($v = 0, 1...n$ are the vibrational bands) as was mentioned earlier. The

peaks representing them were reproduced by Gaussians G1 (443 nm), G2 (449 nm) and G4 (480 nm) as shown in Figure 4.11.

Their kinetic traces displayed a complicated profile as seen in Figure 4.16. An initial fast recovery (see Figure 4.16(b)) with time constant of 6 ps (average of 6, 4 and 7 ps given in Table 4.3) which compared well with those obtained for the early decay in ESA signals signified that the same dynamics were responsible. They also persisted beyond 600 ps indicating that some molecules remained in excited states and thus supporting our earlier assignment of the long live dynamics seen at 467 nm and 496 nm to triplets. The dynamics of these two signals i.e the GSB and ESA were correlated as shown in Figure 4.16(a). Exponential fit on the trace at G2 (449 nm) is shown in Figure 4.16(b).

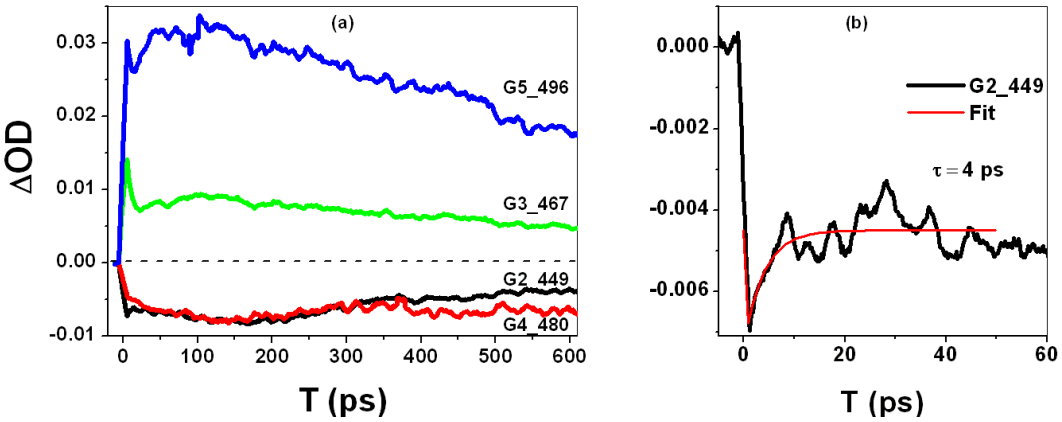

Figure 4.16: The decay kinetic traces for the GSB and ESA signals for the 300 nm thick crystal plotted on the same axes in (a) and single exponential fit applied on the initial dynamics of the GSB signal at 449 nm shown in (b).

Table 4.3: Table of decay time constants for the GSB signals represented in Figure 4.16 for the 300 nm thick crystal.

	GSB		
Gaussian	G1	G2	G4
λ_0 (nm)	443	449	480
τ (ps)	6	4	7

SE signals (G7, G8, G9)

SE signals, which have negative amplitudes in TA spectra as was described earlier, result from photo-induced radiative decay of excited electronic states. They mainly emanate from the vibrationally relaxed first excited singlet state (see Figure 4.14) and have red-shifted peaks relative to those of GSB signals.

The peak representing it in our crystal was that reproduced by Gaussians G7 (538 nm) and G9 (544 nm). The kinetic traces of these Gaussians displayed a decaying emission with a time constant of 10 ps (average of 9ps and 11 ps in Table 4.4) as shown in Figure 4.17(a). Positive amplitude signals (increased absorbance) were also observed after the combined large negative signal had decayed (see

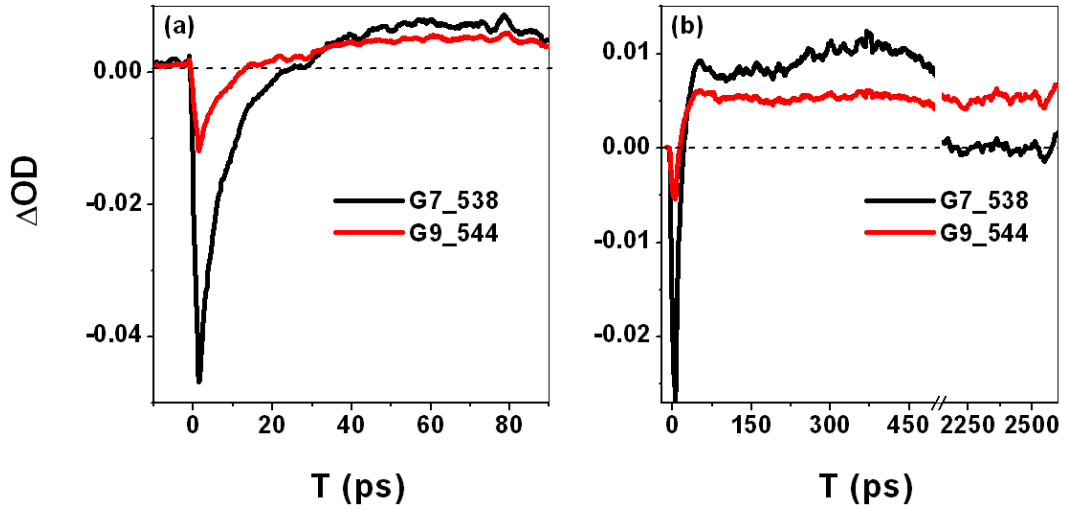

Figure 4.17: The decay kinetic traces for the SE signals for the 300 nm thick crystal displaying an initial rapid emission occurring within the first 20 ps in (a) and (b) decay extending from picoseconds to nanoseconds timescale.

Figure 4.17(b)). The SE signal (the negative amplitude part) was thought to orig-

Table 4.4: Table of decay time constants for the SE signals represented in Figure 4.17(a) for the 300 nm thick crystal.

	SE	
Gaussian	G7	G9
λ_0 (nm)	538	544
τ (ps)	9	11

inate from the low energy Davydov component centered at 520 nm. A similar short lived emission with a time constant of 9.2 ps attributed to a superradiant $S_0 \longleftarrow S_1$ transition was reported earlier in polycrystalline Tc thin films at room temperature [23]. The positive signals resulting after the decay of emission seen in our crystals were thought to be due to absorption by trapped excitons at defect sites. This assignment was based on the fact that no triplet states have been reported at these wavelengths (i.e 538 nm and 540 nm) in literature and the only other probable states displaying long decay times in molecular crystals are defect states. These defects could also arise from a transient structural phase transition.

Excitation of the 300 nm crystal at 387 nm and probe polarized $\perp$ b axis

In chapter 3, Davydov splitting in $S_0 \rightarrow S_1$ transitions of 0.08 eV was measured. This splitting, as was pointed out, resulted from Coulombic interaction between the two differently oriented molecules in Tc unit cell. This was observed with polarized excitation of the crystal i.e using light that was polarized $\parallel$ b and $\perp$ b axis of the ab crystal face. In this studies an attempt was made to determine lifetimes of the two Davydov excitonic states through using probes which were

polarized $\perp$ b and $\parallel$ b axis. In the previous discussion the probe was polarized $\parallel$ b thus interrogating transitions to the low energy Davydov state. The obtained results displayed broad and large amplitude ESA (at 467 nm and 496 nm) and SE (at 540 nm) signals as was seen in Figure 4.9(b). The GSB (at around 443 nm and 482 nm) on the other hand were weak implying that a significant fraction of excitons at these energies decayed. This Davydov state lifetime could not be established precisely. Here we probe the high energy Davydov state with a beam polarized $\perp$ b axis. The same excitation conditions as in above experiment were employed.

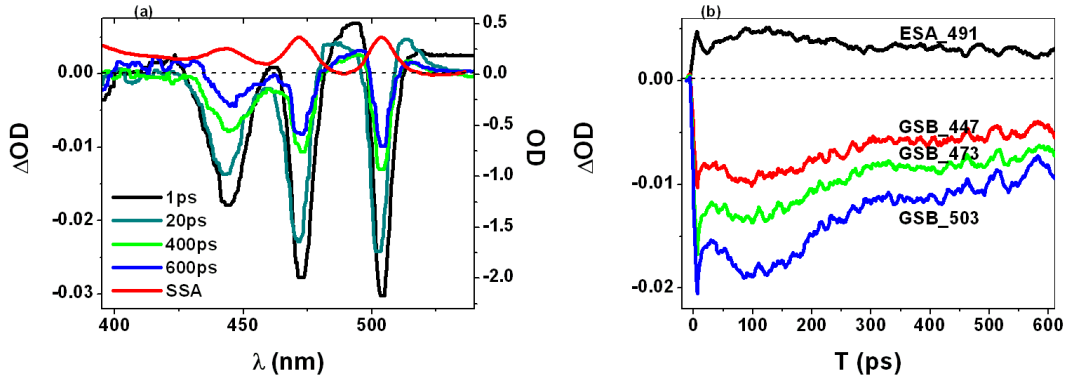

Figure 4.18: (a)The transient absorption spectra of the 300 nm thick Tc crystal excited at 387 nm and probed with $\perp$ b-polarized white light at different times after excitation and with the steady state absorption (SSA) spectra also plotted on the same wavelength axis. The signal was dominated by GSB (at 503 nm, 473 nm, 447 nm) signals. A long living positive signal was also noticed at 491 nm attributed to $T_1 \rightarrow T_n$ absorption. (b) The decay kinetic traces of both the GSB and ESA signals.

The obtained transient spectra was dominated by GSB signals situated at 503 nm, 473 nm and 443 nm as seen in Figure 4.18(a). A positive amplitude peak was also observed at around 491 nm close to where a large ESA signal (at 496 nm) attributed to $T_1 \rightarrow T_n$ transition was observed before in this work with using a probe polarized $\parallel$ b axis. The other ESA peak (due to excited triplet absorption) expected at around 467 nm did not appear in this spectrum.

The large negative amplitude and long living GSB signals implied that majority of the electronic populations at these energies were evolving in higher excited states. The most probable long living excitonic states were triplets. Given that the probed high energy Davydov states in the 0-0, 0-1 and 0-2 vibrational transitions situated at around 503 nm, 473 nm and 443 nm respectively were higher in energy or nearly degenerate with the ME state ($^1(T_1T_1)$) at between 480-498 nm (see Figure 4.14) [33, 42], a rapid singlet fission was highly possible. This then accounted for the large negative amplitude GSB signals. The signal observed at 491 nm (see Figure 4.18(b)) was thought to represent $T_1 \rightarrow T_n$ transitions.

From these results one can conclude that the high energy Davydov states were short-lived (<1ps) as their population was readily distributed to the triplet states.

Excitation of the 300 nm crystal at 530nm

The dynamics in the 300 nm thick crystal were also studied with excitation done at 530 nm which accessed only the S_1 state. The idea was to identify dynamics that were dependent on excitation energy. Pump pulses of duration 30 fs (full-width at half maximum, fwhm), fluence of 665 μJ cm^{-2} and 30 nm bandwidth were used and probed with white light continuum polarized $\parallel b$. With this excitation, singlet fission (SF) will only proceed through thermal activation via multi-exciton (ME) state as was schematically represented in Figure 4.14 [42]. This state is located between 480 nm and 498 nm according to literature [33, 42]. The high energy wing side of the pump pulse extended upto 510 nm which was below this state's energy. A sub-picoseconds rise in the peaks attributed to absorption by excited triplet states $T_1 \rightarrow T_n$ at 467 nm and 496 nm was therefore not expected. A rapid rise at this timescale was previously attributed to direct fission via the ME state of excited S_n states forming triplets [33, 42, 58]. It should be noted that ME state cannot be accessed by a direct absorption of a single photon since such a transition is forbidden due to Pauli principle [42].

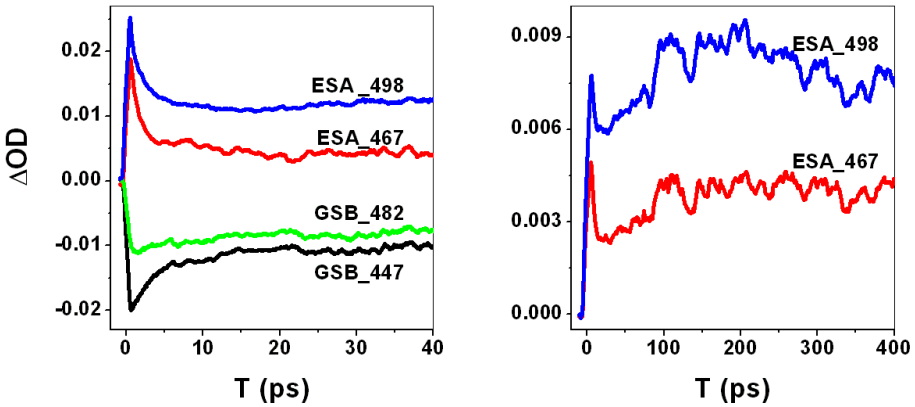

Figure 4.19: The decay kinetic traces of the 300 nm thick crystal excited at 530 nm showing (a) ESA and GSB signal traces within the first 50 ps after excitation showing the initial decay and recovery respectively and (b) ESA signals traces at long times after excitation.

The results obtained with this excitation displayed similar profiles as those given before with a 387 nm excitation (see Figure 4.19). The traces from peaks we attributed to triplets (at 467 nm and 496 nm) did not show an initial rise indicating that they are possibly created rapidly after excitation. This can only be possible if the probe beam coherently excites the vibrational excitons (vibrons) either in the ground state or in S_1 state to S_n. This most likely happens in sub-ps time scale. These states can then fission directly to form triplets as shown in Figure 4.14. Vibrons that are either degenerate, almost degenerate or with slightly higher energies than ME state can also fission rapidly forming triplets [42, 1]. A similar explanation was given by Grumstrup *et al* on dynamics observed in poly-crystalline Tc thin films pumped at 530 nm and probed with both shaped and un-shaped pulses [1]. There was a possibility that ultra-fast inter-system crossing proposed to account for the triplet population observed in solution phase sample was also playing a role in crystals or there was another channel not known yet that was responsible as indicated in studies done by Burdett *et al* [24, 58]. In

reference [24] it was shown through delayed fluorescence measurements at low temperatures and excitation at 530 nm that singlet decay (those created through fusion of triplets) does not depend on excitation energy in contrast to the expectation of the often used simple model of SF where it is assumed to be an activated process.

TA spectroscopy of a 200 nm thick Tc single crystal

Some of the optical properties of the crystal such as absorbance and emission are thickness dependent. A thicker sample will absorb greatly the energy of the exciting field and so making transmission measurements difficult. It will also re-absorb emitted radiation thus compromising the determination of quantum yield in emission measurements.

The transient spectra obtained for the 200 nm thick crystal pumped at 387 nm at room temperature and probed with beam polarized $\parallel$ b axis displayed a profile similar to that of the 300 nm thick crystal indicating that the features were intrinsic (see Figure 4.20). The only difference was the appearance of the GSB signal at 525 nm that was suppressed in the previous sample. This signal overlapped with the SE signal at 533 nm. The defect state signal seen at 538 nm in the previous crystal was missing in the present sample. This further confirmed our assignment since structural defects such as dislocations are expected to be randomly distributed in the crystal.

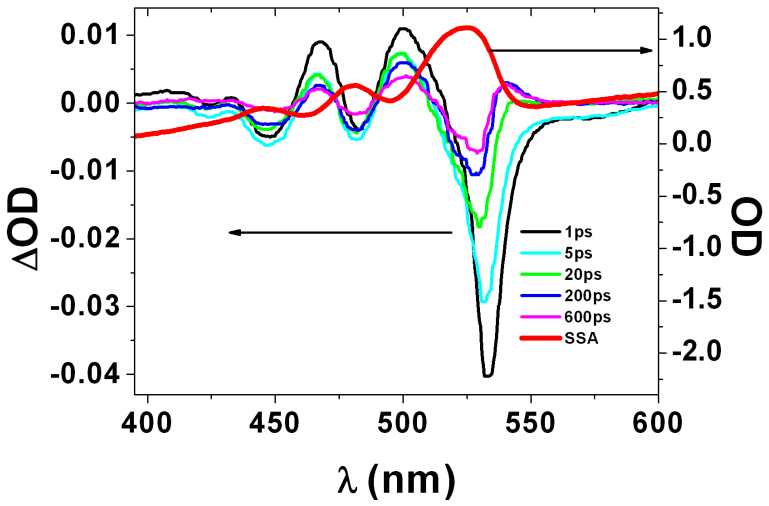

Figure 4.20: The transient absorption spectra of the 200 nm thick Tc crystal probed with a $\parallel$ b polarized white light continuum with the steady state absorption (SSA) spectra plotted in the same wavelength axis. A large negative signal was observed at around 533 nm and the positive signals were at the same positions as those found in the 300 nm thick crystal.

A sum of Gaussians fit was also done in order to deconvolve its transient spectra. The fit obtained reproduced the profile of the spectra as seen in Figure 4.21. The fit parameters used are given in Table 4.5.

The positions of the Gaussian peaks reproducing the GSB and ESA signals were comparable to those obtained for the 300 nm thick crystal discussed in the previous sections. This showed that the deconvolution technique employed here

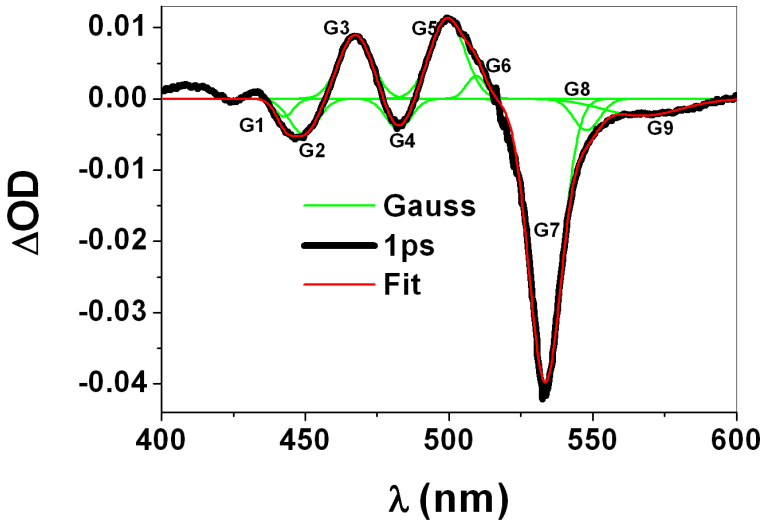

Figure 4.21: The transient absorption spectrum of the 200 nm thick Tc crystal at 1 ps after excitation fitted with a sum of Gaussians. The obtained fit reproduced the general features of the spectrum. The positions of the Gaussian peaks G1 to G9 are also shown.

Table 4.5: The parameters used for the sum of Gaussian fit used in Figure 4.21 for the 200 nm thick crystal. The Gaussians were grouped into GSB, ESA and SE signals as before.

	GSB			ESA			SE		
Gaussian	G1	G2	G4	G3	G5	G6	G7	G8	G9
λ_0 (nm)	443	450	482	468	499	508	533	549	565
σ (nm)	7	11	12	14	13	8	15	9	35
A (a.u)	-0.005	-0.008	-0.012	0.006	0.003	0.034	-0.003	-0.002	-0.002

was robust. The only deviation was in the positions of the Gaussians reproducing the SE signals. No attempt was made here to investigate this descrepancy.

The temporal dynamics of this crystal were similar to those of the previous one (i.e the 300 nm thick crystal) with the GSB and ESA signals displaying an initial recovery and initial decay respectively as seen in Figure 4.22(a). The ESA signals ascribed to triplets seen at 468 nm and 499 nm were also long living as shown in figure 4.22(b). A rapidly decaying emission with a time constant of 7 ps was observed at G7 (533 nm) followed by a slower decay extending upto a bout 225 ps (Figure 4.22 and 4.23).

The extracted decay constants for the initial dynamics (i.e within the first 50 ps as shown in Figure 4.23) ranged between 4 ps and 9 ps (see Table 4.6). These represented the same dynamics explained earlier in this work.

Table 4.6: Decay constants from a single exponential fit on the 200 nm thick crystal's initial decay kinetics i.e within the first 50 ps.

	GSB			ESA			SE		
Gaussian	G1	G2	G4	G3	G5	G6	G7	G8	G9
λ_0 (nm)	443	450	482	468	499	508	533	549	565
τ (ps)	9	5	4	4	3	4	7	9	8

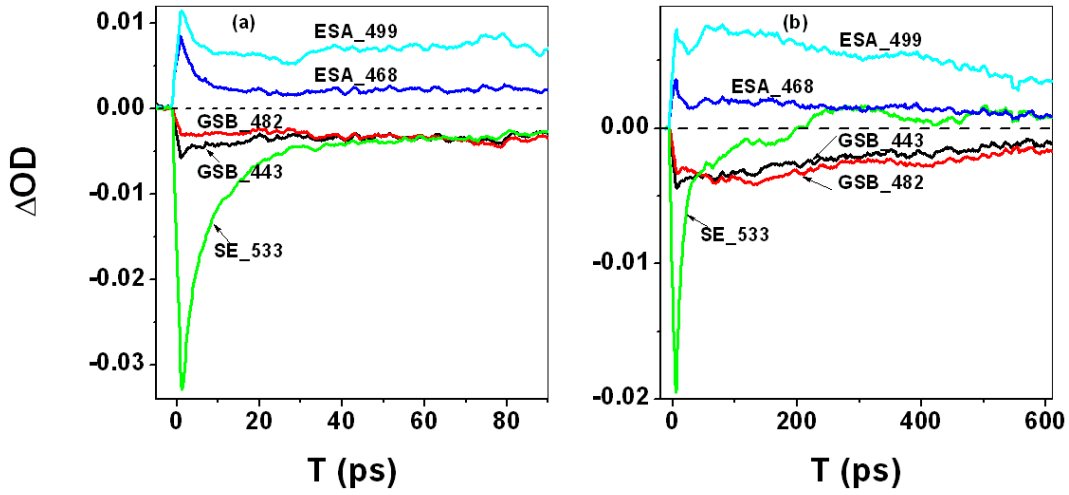

Figure 4.22: The decay kinetic traces for the 200 nm thick crystal. (a)The temporal decay profiles on sub-100 ps after excitation taken with a 0.2 ps probe delay step size and (b) on longer time scale taken wit a 1 ps step size. The ESA signals at 468 nm and 499 nm display a decay extending beyond 600 ps. The SE signal at 533 nm displayed a rapid decay within the first 20 ps.

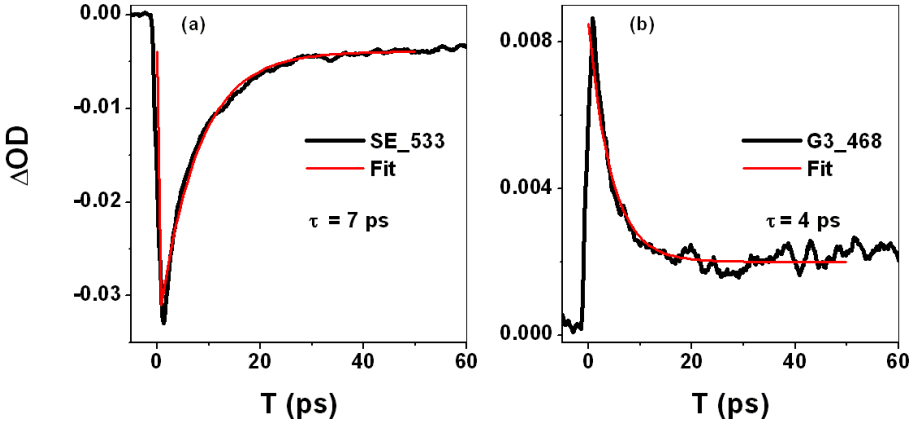

Figure 4.23: Initial rapid decay of (a) emission and (b) ESA fitted with exponential function in the 200 nm thick crystal. The fits were used to extract the decay constants. (a) Displays the fit applied to the SE signal at 533 nm while (b) shows that applied to the ESA signal at 468 nm.

The results obtained with probe polarized $\perp$ b axis were dominated by GSB signals as shown in Figure 4.24. A fairly strong positive signal (ESA) was observed at 491 nm and a week one at 465 nm. These were the same signals assigned to triplets in the previous discussions. The amplitude of the peak at 465 nm was so low that it was never resolved at later times after excitation. The crystal was excited with 170 μW beam power compared to 120 μW used before in order to get a good signal to noise ratio. This increase in excitation strength caused accelerated decay to be observed which stabilized after about 150 ps.

These results from the two crystal samples of different thicknesses served to confirm that the position of the energy levels does not shift with change in thickness. The TA spectrum of the 200 nm thick crystal compared so well with those of polycrystalline Tc thin films obtained elsewhere [23, 24]. The only effect observed with using a thicker sample (300 nm crystal) was the suppression of the GSB signal at 525 nm due to increased absorbance.

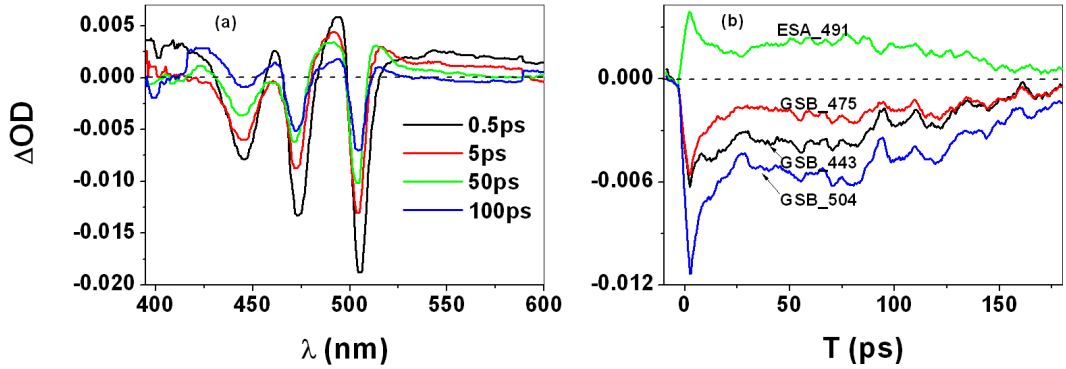

Figure 4.24: TA spectrum of the 200 nm thick crystal with probe polarized $\perp$ b axis of ab face. (a) Spectrum was dominated by GSB signals. An ESA signal was noticed at 491 nm. (b)The decay traces.

The long decay dynamics

We re-visit the long decay dynamics assigned to $T_1 \rightarrow T_n$ transitions in our tetracene crystal samples. Here we are interested in the dynamics responsible for the shape of the kinetic traces which included the observed initial decay, then a rise and finally a long living decay. A global fit was done in order to extract the time constants of these profiles which were then used together with literature values to assign the respective features to a particular physical process in the crystal appropriately. The fit consisted of a multi-exponential function of the form

$$y(t) = G(t) \otimes [\theta(t)\{y_0 + A_1\, exp(-t/\tau_1) + T(t)\}] \tag{4.7}$$

$$T(t) = A_2\{1 + exp(-t/\tau_2)\} + A_3\{1 - exp(-t/\tau_3)\} \tag{4.8}$$

$$G(t) = A\, exp(-(t/\sigma)^2) \tag{4.9}$$

where $G(t)$, σ, $\theta(t)$, A_i, τ_i $(i = 1,2,3)$ represented the Gaussian instrument response function, its width, a step function, amplitudes and time constants respectively. The Gaussian function was convoluted with the product of the step function and the multi-exponential function. The offset y_0 represented yield resulting from sub-ps processes such as direct fission of S_n states. The fit reproduced the general profile of the trace as shown in Figure 4.25 and the results are summarized in Table 4.7.

Table 4.7 provides the fitting parameters. The initial decay that was attributed to exciton-exciton annihilation was represented by the first decay constant τ_1. The value of this constant was kept fixed within the limits of the results presented before in this work. The focus was on the subsequent dynamics i.e the steady rise followed by a slow decay, represented by time constants τ_2 and τ_3 respectively. A value of about 40 ps was found in all the crystal samples irrespective of excitation wavelength as shown in Table 4.7. This signified a feature that was characteristic of the crystal. In other similar TA studies a rise on a 50 ps time scale in single crystals[33] and 37.5 ps in polycrystalline thin films [1] of Tc were observed in absorptive features assigned to $T_1 \rightarrow T_n$ transitions. This dynamic was ascribed to increased triplets yield due to the thermally activated singlet fission (SF). It should be noted that SF time scales measured in TA studies are generally half

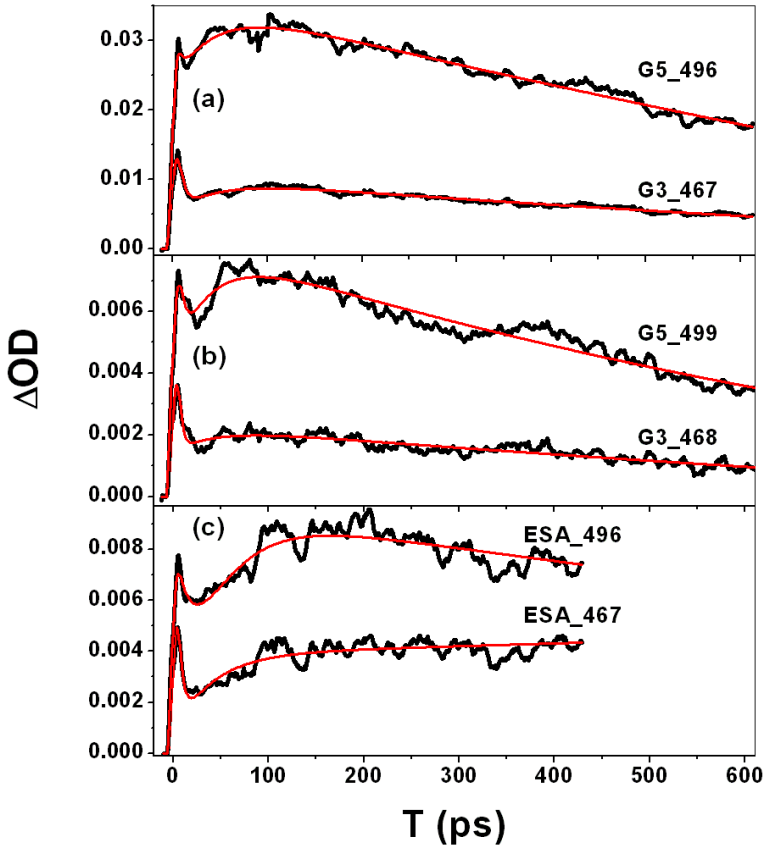

Figure 4.25: The multi-exponential fit on the long decay dynamics of the (a) 300 nm and (b) 200 nm thick crystals excited at 387 nm and (c) the 300 nm thick crystal excited at 530 nm represented by the red line. The probe beam was polarized $\parallel b$ in all these results.

Table 4.7: The long decay dynamics exponential fit results for the crystals excited at 387 nm and at 530 nm. A Gaussian response function of width 200 fs was used.

λ (nm)	S	ESA (nm)	$\tau_1(ps)$	$\tau_2(ps)$	$\tau_3(ps)$	A_1	A_2	A_3
387	300nm	467	6	39	2000	0.089	0.02	-0.097
		496	5	40	3000	0.03	0.04	-0.31
	200nm	468	3	40	2000	0.07	0.006	-0.03
		499	5	37	1000	0.04	0.022	-0.057
530	300nm	467	5	40	5000	0.06	0.015	-0.03
		496	19	41	3000	0.03	0.037	-0.05

those obtained from delayed fluorescence measurements 100 ps [24], 75 ps [1, 45]. This was expected since the former method probes the creation while the latter the annihilation of triplet species.

The long decay life times which is a characteristic of triplet states was reflected by time constant τ_3. It's values were in nanoseconds range and so supporting the results displayed in Figure 4.12.

Results obtained here showed clearly the existence of both short-lived (<20 ps) and long-lived (>2.6 ns) excitonic states. The short-lived states can be utilized in the design of an ultra-fast photo-switch, while the long-lived states which were formed between sub-ps and 40 ps timescales can be utilized in improving the per-

formance of solar cells as was described elsewhere [6, 24, 34, 59]. Briefly, the main problems in semiconductor solar cells is the inability of typical photovoltaic materials to convert a large portion of the solar spectrum into usable energy. Most materials thermalize excess energy above the band gap and those below have no effect and their energy is lost. This limits their power-conversion efficiency averaged over the solar spectrum to a maximum of 33 % - the Shockley-Queisser limit [6, 34, 59]. This limitation can be overcome by using materials exhibiting exciton fission, like tetracene, where multiple electron-hole pairs - the triplet excitons - are produced from a single photon. The electrons or holes in the triplet excitons can then be harvested with a suitable holes conductor or acceptor. The rapidity with which singlet fission occur in the samples investigated here ($\leq$40 ps) allow it to compete with other relaxation processes.

The potential utilization of the results obtained here are therefore immense. Besides, the method of preparation of thin free standing tetracene single crystals can be applied in other polyacenes.

5. Conclusions

Conjugated organic semiconductors have in recent years witnessed an increased academic and industrial interest due to their appealing properties and promise to replace their expensive inorganic counterparts in device applications. Devices such as organic light emitting diodes (OLED), organic field-effect transistors (OFET), organic solar cells (OSC) among others based on them have been demonstrated. In order to optimally utilize their properties in these technologies it is important to understand both the nature of photogenerated states and their relaxation dynamics. Towards this end we investigated one of the promising candidates, tetracene. This material has immense absorbance in the visible regime of the electromagnetic spectrum. Any optical transmission measurements on their single crystals therefore required nanometer thick samples. This explains why it is rare to find steady state and transient absorption spectroscopy measurements on single crystals in literature. Using microtome apparatus we were able to cut the provided thick ($\approx 500\ \mu$m) sublimation grown crystal platelets obtaining 200 nm, 300 nm and 500 nm thick single crystals supported on a copper wire mesh with squares of dimensions 150 μm.

The energy positions of tetracene's excitonic states are not well understood and the reported values often depend on the sample preparation history and experimental conditions. Steady state absorption measurements done in this work at room temperature (300 K) on the crystals revealed two excitonic states with orthogonally polarized ($\backsimeq 90^o$) optical transitions. The transition polarized $\perp$ b-axis (high energy Davydov band) of the ab crystal face had the 0-0, 0-1, and 0-2 vibrational bands centered at 503 nm, 472 nm and 443 nm respectively. The $\parallel$ b-axis (low energy Davydov band) transition on the other hand had their 0-0, 0-1, and 0-2 vibrational bands centered at 520 nm, 478 nm and 444 nm respectively. From these two states, a Davydov splitting energy of between 0.08 eV and 0.12 eV was determined and compared well with experimentally and theoretically determined literature values and thus confirming similarities in the samples. The crystal spectrum was also red-shifted with respect to the solution spectrum and there was a solution-to-crystal shift energy of 0.15 eV and 0.23 eV in the 0-0 vibrational bands of the high and low energy Davydov components respectively.

The broad aim of femtosecond transient absorption spectroscopy measurements was to reveal positions of states other than S_1, which steady state measurements provided, and their relaxation dynamics. Besides, there were few such measurements done on tetracene single crystals. Excited state absorption (ESA) signals play a key role in tetracene dissolved in toluene solvent as was revealed by a large positive signal in its transient spectrum. Superimposed on top of this signal were negative ground state bleach signals. Signatures of excited triplet absorption were also seen 20 ps after excitation at 465 nm. This unexpected feature

in the stated timescale was proposed here for the first time to result from fast inter-system crossing (ISC) facilitated by the position of the second excited triplet state being energetically below the first excited singlet state S_1. This triplet formation was confirmed by probing the excited sample at 10 ns. The transient absorption spectra obtained from single crystals were complicated by overlapping GSB and ESA signals which frustrated efforts to interpret them in other studies. Here we employed a robust deconvolution technique involving use of sum of Gaussians fit. From this technique positive signals attributable to absorption by T_1 state were identified from the long living peaks on the transient absorption spectra at 467 nm and 496 nm. The population of T_1 state occurred from fission of not only the lowest excited singled state $S_1 \rightarrow 2T_1$ but also of the higher-lying singlet states $S_n \rightarrow 2T_1$ in 40 ps and sub-picoseconds time scales respectively at room temperature. These states seen through $T_1 \rightarrow T_n$ transition bands displayed a decay extending beyond 2.6 ns. The attribution of the peak observed at 467 nm was done for the first time in this studies but the one at 496 nm had been done somewhere else. The rapid generation of triplet excitons which apart from having long decay lifetimes also have large diffusion lengths can be utilized in solar cells where the electrons and holes can be harvested with help of suitable acceptor materials. There was also an emission on a time scale of about 10 ps which can be applied in the design of an ultra-fast photo-switch. The rapid generation of triplets was independent of excitation energy as was found out from comparing excitation done at 387 nm and 530 nm corresponding to S_n and S_1 excitation respectively. Triplet population in the crystals occur mainly from the high energy Davydov state as observed from the large negative ground state bleach signals obtained with probe field polarized $\perp$ b-axis compared with those with field polarized $\parallel$ b of the ab face of the unit cell.

List of References

[1] Grumstrup, E.M., Johnson, J.C. and Damrauer, N.H.: Enhanced triplet formation in polycrystalline tetracene films by femtosecond optical-pulse shaping. *Physical Review Letters*, vol. 105, pp. 257403–4, 2010.

[2] Takahashi, T., Takenobu, T., Takeya, J. and Iwasa, Y.: Ambipolar light-emitting transistors of a tetracene single crystal. *Advanced Functional Materials*, vol. 17, pp. 1623–1628, 2007.

[3] Jiang, L., Dong, H. and Hu, W.: Organic single crystal field-effect transistors: advances and perspectives. *Journal of Materials Chemistry*, vol. 20, pp. 4994–5007, 2010.

[4] de Boer, R.W.I., Klapwijk, T.M. and Morpurgo, A.F.: Field-effect transistors on tetracene single crystals. *Appllied Physics Letters*, vol. 83, pp. 4345–4347, 2003.

[5] Xia, Y., Kalihari, V., Frisbiea, C.D., Oh, N.K. and Rogers, J.A.: Tetracene air-gap single-crystal field-effect transistors. *Applied Physics Letters*, vol. 90, p. 162106, 2007.

[6] Paci, I., Johnson, J.C., Chen, X., Rana, G., Popovic, D., David, D.E., Nozik, A.J., Ratner, M.A. and Michl, J.: Singlet fission for dye-sensitized solar cells: Can a suitable sensitizer be found? *Journal of American Chemical Society*, vol. 128, pp. 16546–16553, 2006.

[7] Hanna, M.C. and Nozik, A.J.: Solar conversion efficiency of photovoltaic and photoelectrolysis cells with carrier multiplication absorbers. *Journal of Applied Physics*, vol. 100, p. 074510, 2006.

[8] Chu, C.-W., Shao, Y., Shrotriya, V. and Yanga, Y.: Efficient photovoltaic energy conversion in tetracene-c60 based heterojunctions. *Applied Physics Letters*, vol. 86, p. 243506, 2005.

[9] Hochstrasser, R.M.: Spectroscopy at a stretch. *NATURE*, vol. 434, p. 570, MARCH 2005.

[10] Engel, G.S., Calhoun, T.R., Read, E.L., Ahn, T.-K., Mancal, T., Cheng, Y.-C., Blankenship, R.E. and Fleming, G.R.: Evidence for wavelike energy transfer through quantum coherence in photosynthetic systems. *NATURE*, vol. 446, pp. 782–786, 2007.

[11] Yuan-Chung, C. and Fleming, R.G.: Dynamics of light harvesting in photosynthesis. *Annual Review of Physical Chemistry*, vol. 60, no. 1, pp. 241–262, 2009.

[12] Vygintas, J.: *Study of Triplet Exciton Dynamics in Small Organic Molecule Films Using Time Resolved Optical Spectroscopy*. Doctoral thesis, Durham University, http://etheses.dur.ac.uk/495/, 2010.

[13] Schwoerer, M. and Wolf, H.C.: *Organic molecular solids*. Wiley-VCH Verlag GmbH and Co. KGaA, Weinheim, 2007.

[14] Tavazzi, S., Raimondo, L., Silvestri, L., Spearman, P., Camposeo, A., Polo, M. and Pisignano, D.: Dielectric tensor of tetracene single crystals: The effect of anisotropy on polarized absorption and emission spectra. *The Journal of Chemical Physics*, vol. 128, p. 154709, 2008.

[15] Firouzi, R. and Zahedi, M.: Polyacenes electronic properties and their dependence on molecular size. *Journal of Molecular Structure*, vol. THEOCHEM 862, pp. 7–15, 2008.

[16] Yamagata, H., Norton, J., Hontz, E., Olivier, Y., Beljonne, D., Braedas, J.L., Silbey, R.J. and Spano, F.C.: The nature of singlet excitons in oligoacene molecular crystals. *The Journal of Chemical Physics*, vol. 134, p. 204703, 2011.

[17] Kena-Cohen, S. and Forrest, S.R.: Giant davydov splitting of the lower polariton branch in a polycrystalline tetracene microcavity. *Physical Review B*, vol. 77, p. 073205, 2008.

[18] Zhu, X., Yang, Q. and Muntwiler, M.: Charge-transfer excitons at organic semiconductor surfaces and interfaces. *Accounts of Chemical Research*, vol. 42, no. 11, pp. 1779–1787, 2009.

[19] Voigt, M., Langner, A., Schouwink, P., Lupton, J.M., Mahrt, R.F. and Sokolowski, M.: Picosecond time resolved photoluminescence spectroscopy of a tetracene film on highly oriented pyrolytic graphite: Dynamical relaxation, trap emission, and superradiance. *The Journal of Chemical Physics*, vol. 127, p. 114705, 2007.

[20] Menzel, E.R.: Interaction of light with molecules- an overview. *Applied Spectroscopy Reviews*, vol. 34, no. 4, pp. 209–247, 1999.

[21] West, B.A., Womick, J.M., McNeil, L.E., Tan, K.J. and Moran, A.M.: Ultrafast dynamics of frenkel excitons in tetracene and rubrene single crystals. *Journal of Physical Chemistry, C*, vol. 114, pp. 10580 –10591, 2010.

[22] Pope, M.: Charge-transfer exciton state, ionic energy levels, and delayed fluorescence in anthracene. *Molecular Crystals*, vol. 4, pp. 183–190, 1968.

[23] Burdett, J.J., Mueller, A.M., Gosztola, D. and Bardeen, C.J.: Excited state dynamics in solid and monomeric tetracene: The roles of superradiance and exciton fission. *The Journal of Chemical Physics*, vol. 133, p. 144506, 2010.

[24] Burdett, J.J., Gosztola, D. and Bardeen, C.J.: The dependence of singlet exciton relaxation on excitation density and temperature in polycrystalline tetracene thin films: Kinetic evidence for a dark intermediate state and implications for singlet fission. *The Journal of Chemical Physics*, vol. 135, pp. 214508–1–10, 2011.

[25] Fleming, G.R., Miller, D.P., Morris, G.C. and Robinson, G.W.: Exciton fission and annihilation in crystalline tetracene. *Australian Journal of Chemistry*, vol. 30, pp. 2353–2359, 1977.

[26] Muller, A.M., Avlasevich, Y.S., Muellen, K. and Bardeen, C.J.: Evidence of exciton fission and fussion in covalently linked tetracene dimer. *Chemical Physics letters*, vol. 421, pp. 518–522, 2006.

[27] Vaubel, G. and Baessler, H.: Excitation spectrum of crystalline tetracene fluorescence: A probe for optically-induced singlet-exciton fission. *Molecular crystals and liquid crystals*, vol. 15, pp. 15–25, 1971.

[28] Vaubel, G. and Baessler, H.: Diffusion of singlet excitons in tetracene crystals. *Molecular crystals and liquid crystals*, vol. 12, pp. 47–56, 1970.

[29] Pope, M., Burgos, J. and Giachino, J.: Charge-transfer exciton state and energy levels in tetracene crystal. *Journal of Chemical Physics*, vol. 43, no. 8, p. 3367, 1965.

[30] Arden, W., Kotant, M. and Peter, L.M.: Triplet exciton decay process in crystalline tetracene. *Physica Status Solidi (b)*, vol. 75, pp. 621–631, 1976.

[31] Schlosser, W.D. and Philpott, R.M.: Singlet excitons in crystaliline naphthalene, anthracene, tetracene and pentcene. *Chemical Physics*, vol. 49, pp. 181–199, 1980.

[32] Tavazzi, S., Campione, M., Laicini, M., Raimondo, L., Borghesi, A. and Spearman, P.: Measured davydov splitting in oligothiophene crystals. *The Journal of Chemical Physics*, vol. 124, p. 194710, 2006.

[33] Thorsmolle, V.K., Averitt, R.D., Demsar, J., Smith, D.L., Tretiak, S., Martin, R.L., Chi, X., Crone, B.K., Ramirez, A.P. and J.Taylo, A.: Morphology effectively controls singlet-triplet exciton relaxation and charge transport in organic semiconductors. *Physical Review Letters*, vol. 102, pp. 017401–4, 2009.

[34] Greyson, E.C., Stepp, B.R., Chen, X., Schwerin, A.F., Paci, I., Smith, M.B., Akdag, A., Johnson, J.C., Arthur, Nozik, J., Michl, J. and Ratner, M.A.: Singlet exciton fission for solar cell applications: Energy aspects of interchromophore coupling. *Journal of Physical Chemistry, B*, vol. 114, pp. 14223–14232, 2010.

[35] Davydov, A.S.: The theory of molecular excitons. *Soviet Physics Uspekhi*, vol. 82, pp. 393–448, 1964.

[36] Ginsberg, N.S., Cheng, Y.-C. and Fleming, G.R.: Two-dimensional electronic spectroscopy of molecular aggregates. *Accounts of Chemical Research*, vol. 42, no. 9, pp. 1352–1363, 2009.

[37] Kasha, M., Rawls, H.R. and El-Bayoum, M.A.: The exciton model in molecular spectroscopy. Institute of Molecular Biophysics and Department of Chemistry, Florida State University, Tallahassee, Florida.

[38] Hesse, R., Hofberger, W. and Baessler, H.: Absorption spectra of disordered solid tetracene and pentacene. *Chemical Physics*, vol. 49, pp. 201–211, 1980.

[39] Smith, M.B. and Michl, J.: Singlet fission. *Chemical Review*, vol. 110, pp. 6891–6936, 2010.

[40] Johnson, J., Frank, A.J., Neale, N.R., Zhu, K., Nozik, A.J. and Michl, J.: New directions for efficient solar water splitting based on two photosystems and singlet fission chromophores. In: *2011 Annual Merit Review Meeting*. DOE Hydrogen and Fuel Cells Program, USA, 2011.

[41] Chan, W.-L., Ligges, M., Jailaubekov, A., Kaake, L., Miaja-Avila, L. and Zhu, X.-Y.: Observing the multiexciton state in singlet fission and ensuing ultrafast multielectron transfer. *Science*, vol. 334, pp. 1541–1545, 2011.

[42] Zimmerman, P.M., Bell, F., Casanova, D. and Head-Gordon, M.: Mechanism for singlet fission in pentacene and tetracene: From single exciton to two triplets. *Journal of the American Chemical Society*, vol. 133, pp. 19944–19952, 2011.

[43] Groff, R.P., Avakian, P. and Merrifield, R.E.: Coexistence of exciton fission and fussion in tetracene crystals. *Physical Review B*, vol. 1, no. 2, pp. 815–817, 1970.

[44] Camposeo, A., Polo, M., Tavazzi, S., Silvestri, L., Spearman, P. and R. Cingolani, a.D.P.: Polarized superradiance from delocalized exciton transitions in tetracene single crystals. *Physical Review B*, vol. 81, p. 033306, 2010.

[45] Lim, S.-H., Bjorklund, T.G., Spano, F.C. and Bardeen, C.J.: Exciton delocalization and superradiance in tetracene thin films and nanoaggregates. *Physical Review Letters*, vol. 92, no. 10, pp. 1074021–1074024, 2004.

[46] Bensasson, R. and Land, E.J.: Triplet-triplet extinction coefficients via energy transfer. *Transactions of the Faraday Society*, vol. 67, pp. 1904–1915, 1971.

[47] Liu, K.-L., Chen, Y.-T., Lin, H.-H., Hsu, C.-S., Chang, H.-W. and Chen, I.-C.: Dynamics of the excited states of p-terphenyl and tetracene: Solute-solvent interaction. *Journal of physical chemistry, C*, vol. 115, pp. 22578–22586, 2011.

[48] Fournie, G., Dupuy, F., Martinad, M., Nouchi, G. and Turlet, J.M.: Autoassociation of tetracene in solution. *Chemical Physics Letters*, vol. 15, pp. 332–335, 1972.

[49] Pavlopoulos, T.G.: Measurement of triplet-triplet absorption spectrum of tetracene using cw argon laser excitation. *The Journal of chemical physics*, vol. 56, 1972.

[50] Geacintov, N., Pope, M. and Kallman, H.: Photogeneration of charge carriers in tetracene. *Journal of chemical Physics*, vol. 45, no. 7, p. 2639, 1966.

[51] Berera, R., van Grondelle, R. and Kennis, J.T.M.: Ultrafast transient absorption spectroscopy: principles and application to photosynthetic systems. *Photosynth Res*, vol. 101, pp. 105–118, 2009.

[52] Megerle, U., Pugliesi, I., Schriever, C., Sailer, C.F. and Riedle, E.: Sub-50 fs broadband absorption spectroscopy with tunable excitation: putting the analysis of ultrafast molecular dynamics on solid ground. *Applied Physics B: Lasers and Optics*, vol. 96, pp. 215–231, 2009.

[53] Riedle, E., Beutter, M., Lochbrunner, S., Piel, J., Schenkl, S., Spoerlein, S. and Zinth, W.: Generation of 10 to 50 fs pulses tunable through all of the visible and the nir. *Applied Physics B*, vol. 71, pp. 457–465, 2000.

[54] Cerullo, G. and Silvestri, S.D.: Ultrafast optical parametric amplifiers. *Review of scientific instruments*, vol. 74, pp. 1–18, 2003.

[55] Wilhelm, T., Piel, J. and Riedle, E.: Sub-20-fs pulses tunable across the visible from a blue-pumped single-pass noncollinear parametric converter. *Optics Letters*, vol. 22, pp. 1494–1496, 1997.

[56] Brodeur, A. and Chin, S.L.: Ultrafast white-light continuum generation and self-focusing in transparent condensed media. *Journal of Optical Society of America, B*, vol. 16, pp. 637–650, 1999.

[57] Kozma, I.Z., Baum, P., Schmidhammer, U., Lochbrunner, S. and Riedle, E.: Compact autocorrelator for the online measurement of tunable 10 femtosecond pulses. *Review of Scientific instruments*, vol. 75, pp. 2323–2327, 2004.

[58] Burdett, J.J. and Bardeen, C.J.: Quantum beats in crystalline tetracene delayed fluorescence due to triplet pair coherences produced by direct singlet fission. *Journal of the American Chemical Society*, vol. 134, pp. 8597–8607, 2012.

[59] Miller, J.: Multiple exciton generation enhances a working solar cell. *Physics Today*, vol. 65, pp. 17–19, 2012.

A. Appendix

Absorption cross section $\sigma(\lambda)$

Here we show how the values stated in this thesis were obtained which include the absorption cross section $\sigma(\lambda)$ and the number of molecules excited in both the solution and the crystals investigated. The molar mass (MM) of tetracene, $C_{18}H_{12}$ was found from

$$MM = (12.01 \times 18) + (1.0079 \times 12) = 228 \text{ g/mole}. \tag{A.1}$$

The Avogadros No. $= 6.626 \times 10^{23}$ molecules / mole.
Mass of tetracene dissolved in toluene solvent $M = 4.0 \times 10^{-4}$ g.
Volume of Tc solution $V = 0.37$ cm^3.
Length of cuvette $= 0.1$ cm.
Concentration of tetracene in toluene solvent in the cuvette was determined from,

$$c = \frac{M}{V \times MM} = \frac{4 \times 10^{-4}}{0.37 \times 228} = 4.7 \times 10^{-6} \text{ moles / cm}^3. \tag{A.2}$$

This was then expressed in terms of number of tetracene molecules per unit volume obtaining

$$c_{sol} = (6.626 \times 10^{23}) \times (4.7 \times 10^{-6}) = 3.14 \times 10^{18} \text{ molecules / cm}^3. \tag{A.3}$$

Since the laser beam (white light continuum) was shone on a diameter of ≈ 0.02 cm, then the volume excited was

$$V_{exc}^{sol} = \pi \times (0.01)^2 \times 0.1 = 3.14 \times 10^{-5} \text{ cm}^3 \tag{A.4}$$

and the number of tetracene molecules excited N_{Tc}^{sol} was then

$$N_{Tc}^{sol} = V_{exc}^{sol} \times c_{sol} = 3.14 \times 10^{-5} \times 3.14 \times 10^{18} = 9.9 \times 10^{13} \text{ molecules}. \tag{A.5}$$

The absorbance value of 0.25 at 474 nm in tetracene dissolved in toluene given in Table 3.1 was obtained from exciting a fraction ($\frac{3.14 \times 10^{-5}}{0.37}$) of the volume in the cuvette . Nevertheless, if we consider that entire volume was excited, we can estimate absorption cross section $\sigma(\lambda)$ as

$$\sigma(\lambda) = \frac{OD}{c_{sol} \times l} = \frac{0.25}{(3.14 \times 10^{18}) \times 0.1} = 8.0 \times 10^{-19} \text{ cm}^2\text{molecule}^{-1}. \tag{A.6}$$

Required tetracene crystal thickness

Now when determining the appropriate thickness of tetracene crystal required to obtain an absorbance of 0.25 similar to that in solution at 474 nm, we need to first determine the number of molecules in a unit volume. Given that the volume of tetracene unit cell is 583 $\times 10^{-24}$cm^3 and that there are two molecules per unit cell then we get

$$c_{crystal} = \frac{2}{583 \times 10^{-24}} = 3.4 \times 10^{21} \text{ (molecules) cm}^{-3} \tag{A.7}$$

The thickness which can give absorbance of 0.25 can be obtained from

$$l_{crystal} = \frac{OD}{\sigma(\lambda) \times c_{crystal}} = \frac{0.25}{(8.0 \times 10^{-19}) \times 3.4 \times 10^{21}} = 920 \text{ nm} \tag{A.8}$$

The number of molecules excited $N_{Tc}^{crystal}$ in the crystal

Given that the excitation spot diameter was 0.02 cm, one can estimate the number of molecules excited in the 200 nm, 300 nm and 500 nm thick samples from

$$N_{Tc}^{crystal} = \pi r^2 l c_{crystal} \tag{A.9}$$

$$N_{Tc}^{crystal,200nm} = 2.1 \times 10^{13} \text{ molecules} \tag{A.10}$$

$$N_{Tc}^{crystal,300nm} = 3.2 \times 10^{13} \text{ molecules} \tag{A.11}$$

$$N_{Tc}^{crystal,500nm} = 5.3 \times 10^{13} \text{ molecules} \tag{A.12}$$